The Pennsylvania State University

The Graduate School

SUSPENDED SEDIMENT CONCENTRATION PREDICTION USING DEEP LEARNING ACROSS THE CONTIGUOUS UNITED STATES

A Thesis in

Civil Engineering

by

Piyaphat Chaemchuen

Submitted in Partial Fulfillment
of the Requirements
for the Degree of

Master of Science

August 2022

The thesis of Piyaphat Chaemchuen was reviewed and approved by the following:

Chaopeng Shen
Associate Professor of Civil and Environmental Engineering
Thesis Advisor

Li Li
Professor of Civil and Environmental Engineering

Xiaofeng Liu
Associate Professor of Civil and Environmental Engineering

Patrick Fox
John A. and Harriette K. Shaw Professor
Head of the Department of Civil and Environmental Engineering

ABSTRACT

To reconcile the need to sustain river communities, water quality, and ecosystem services against the needs for water supply, daily usage, and power generation, to name a few, extensive understanding and accurate sediment estimates are required. However, sediment's nonlinearity and complex hysteresis characteristics make sediment prediction challenging. Furthermore, most of the past studies have focused solely on a local scale and simply ignored human-induced disturbances, land cover status, geological properties, etc. There lacked a systematic way to predict sediment contributions at large scales and high accuracy.

This study developed models based on long short-term memory (LSTM) deep networks to predict SSC over 377 sites across the Contiguous United States (CONUS) with hydrometeorological forcing datasets from the DAYMET, Daily Surface Weather, and Climatological Summaries (Jan 1980 – Dec 2019), streamflow from USGS, United States Geological Survey, sediment-related static attributes from GAGES-II, Geospatial Attributes of Gages for Evaluating Streamflow or non-sediment-related static attributes (simulated random vectors) as inputs. The model has been trained either basin by basin (called the local model) or for the entire CONUS (call the Whole-CONUS model) with the optimal period to cope with data availability and variations of each basin.

The local models for 377 sites across the CONUS show much superior prediction performance compared to the Whole-CONUS model, in terms of a median of the Nash-Sutcliffe Error (NSE), Pearson's Correlation Coefficient (R), Coefficient of Determination (R2), Root Mean Square Error (RMSE, [mg/L]), and Bias [mg/L] of all sites equal to 0.687, 0.868, 0.727, 67.295, 1.379 respectively in testing. The result from the Whole-CONUS from all sites training (377 sites) with sediment-related attributes shows relatively lower statistical metrics (0.596, 0.806, 0.645, 79.303, and -3.403. for Nash-Sutcliffe Error (NSE), Pearson's Correlation Coefficient (R), Coefficient of Determination (R2), Root Mean Squared Error, and Bias respectively) and with random vector attributes ((0.508, 0.788, 0.621, 92.186, and -4.507. for Nash-Sutcliffe Error (NSE), Pearson's Correlation Coefficient (R), Coefficient of Determination (R2), Root Mean Squared Error, and Bias respectively). For ungauged site experiment, the Whole-CONUS with 284 training sites perform a satisfying performance in Suspended Sediment Concentration prediction with a 0.591, 0.810, 0.651, 84.598, and -1.669 for Nash-Sutcliffe Error (NSE), Pearson's Correlation Coefficient (R), Coefficient of Determination (R2), Root Mean Squared Error, and Bias respectively. With a Whole-CONUS that has been trained with 284 basins, it can predict the 93-ungauged sites with satisfactory performance (0.521, 0.865, 0.749, 79.129, and -0.211 for Nash-Sutcliffe Error (NSE), Pearson's Correlation Coefficient (R), Coefficient of Determination (R2), Root Mean Squared Error, and Bias)

The results from this study suggest that on gauged sites, the locally-trained LSTM model is the best approach to estimate the SSC time series. In the ungauged sites, the Whole-CONUS can be considered an acceptable approach for expanding the availability of SSC data. The Whole-CONUS model has been trained either with sediment-related or with non-sediment-related attributes higher overall performance when the model has been trained with the sediment-related attributes. The Whole-CONUS model captures the (imperfect) relationships between sediment-related attributes and sediment dynamics, exposing the spatial heterogeneity of SSC characteristics (higher overall performance from the Local-CONUS model compared to the Whole-CONUS model) that require more descriptors to overcome the interconnectedness and the heterogeneous characteristics. Future work should seek these critical inputs to improve the Whole-CONUS model, allowing us to simulate sediment at large scales with high accuracy.

TABLE OF CONTENTS

LIST OF FIGURES

LIST OF TABLES

ACKNOWLEDGEMENTS

My sense of urgency, perseverance, diligence, and love from my mom made this work presented in this research possible.

I want to thank my advisor, Dr. Chaopeng Shen, for his support in every aspect since the first day of knowing him. Dr. Shen provided critical advice regarding research processes, flow designs, troubleshooting bugs, to name a few, etc. Additionally, I would like to thank all folks in the Multiscale Hydrology, Processes, and Intelligence group: JT, DP, Tadd, Farshid, and Doaa. They helped answer questions and were mental supporters.

I want to thank Dr. Zhi Wei, Dr. Elizabeth Boyer, and Gary Shenk for all their comments, troubles shooting ideas, and attention every month of our meeting. Furthermore, I would like to express my tremendous gratitude to my thesis committee, Dr. Li Li and Dr. Xiaofeng Liu, for their suggestions, questions, and overall attention to our research. The questions they asked elevate this research to another level of this thesis work.

Thank you, Lois, Pluem (Peter), Arthur, Gwad, Fern, Ploy, and Orochimaru (my cat) for being my mental supporters when I was feeling low.

All funding to subsidize Piyaphat Chaemchuen comes from the Thai people's taxes. All results and knowledge that have been gained from this research are for them and their younger generations.

Chapter 1

Introduction

Suspended Sediment regimes and Why Do We Need Accurate Suspended Sediment Concentration Modeling?

Riverscapes around the globe are experiencing rapid and tremendous modifications due to human-induced activities (Peipoch et al., 2015; Wohl et al., 2015). Such modifications as river fragmentation, land-use changes, and riparian invasion, to name a few, interrupt both direct and indirect present suspended sediment regimes (Heathcote, 2009; Wohl et al., 2015). The interrupted regimes can directly impact biota, or directly impact their physical habitats, which results in effects on biota (EPA (2003)).

The term "suspended sediment" refers to sediment particles in a water body, which are fine-grained to the point that turbulent eddies are able to outweigh the settling of the sediment particles and carry them along with the fluid (Parson et at., 2015).

Suspended sediments are vital to rivers' aquatic ecosystem and environmental health in myriad ways. Salmonids, for example, can be sensitive to excess fine sediment in the bed, and the aquatic species requires suspended sediment in a suitable size range and concentration for spawning (Newcombe and MacDonald 1991; Jones et al., 2011; Newcombe and MacDonald 2011; Riebe et al., 2014). Also, suspended sediments are geomorphologically and dynamically related to processes in river channel systems; lacking suspended sediment supply can lead to catastrophic losses (Panek (2020)). On the other hand, an excessive amount of suspended sediment can be a harmful result of eutrophic conditions, leading to the losses of aquatic species and freshwater quality (Lemley and Adams (2019)).

Sediments, still, are often considered a minor variable in the river system as traditional river management tends to put a lot of emphasis on the flow regime at the expense of the sediment regime (Wohl et al., 2015). Also, the modeling communities as well that emphasize flow modeling for reasons which are discussed more in the sub-chapter topic ahead.

Accurate suspended sediment modeling will allow engineers, scientists, ecologists, hydrologists, landscape architects, and other natural resources-related professionals to understand and cope with the dynamics, complexity, and non-linearity of the sediment realm to create a new sustainable resources management paradigm for river conservation and restoration, before the river ecosystem is annihilated and altered to irreversible regimes.

From past to present, efforts on sediment predictions

Sediment modeling, which has been primarily done in suspended sediment flux and concentration terms, is still challenging for two main reasons.

First, suspended sediment concentration (SSC) is heavily influenced by diverse, dynamic hydrologic inputs such as precipitation, soil erosion processes, riverine sediment processes (scouring or deposition), topography, land cover, anthropogenic activities like management practices, and more (Leopold et al., 1992; Bhagat, Tung, and Yaseen 2020; Taher and Hamideh, 2020; Wohl, 2020). Spatial and temporal variations of those factors make the sediment realm complex, non-stationary, and nonlinear (Afan et al., 2014; Nourani et al., 2014).

Second, the determination of SSC in rivers is time-consuming and expensive, making long-term SSC observations scarce. This in turn makes it more difficult to assess the impacts of human disturbance. For example, whereas over 20,000 US Geological Survey gaging stations have long-term (i.e., longer than five years) historical datasets of streamflow discharge in the United States, only around 1500 sites have more than five years' worth of suspended-sediment concentration data (Austin et al., 2017). Long-term data sets are necessary for characterizing the magnitude, frequency, duration, timing or predictability, and rate of change or flashiness of sediment transport for different regions and rivers (Poff et al. 1997), leading to even more challenges in forecasting (Fatih et al., 2020).

Traditionally, engineers use the sediment rating curve, a sediment-discharge relation curve. However, utilizing a log-log rating curve, the rating curve approach, or the duration curve method, can underestimate sediment loads by up to 50%, even when the whole time series of concentration is known (Ferguson 1980).

For decades, many types of suspended sediment models have been proposed across various scales (Cigizoglu (2004); Agarwal et al., 2005; Kisi 2005; Cigizoglu and Alp (2006); Alp and Cigizoglu (2007); Lohani et al., 2007; Francke et al., 2008; Kisi 2008; Jothiprakash and Garg (2009); Rajaee et al., 2009; Firat and Gungor 2010; Melesse et al., 2011; Mustafa et al., 2012; Singh et al., 2013; Afan et al., 2014; Mustafa and Isa (2014); Olyaie et al., 2014; Kumar et al., 2016; Kaveh et al., 2017; Tasar et al., 2017; Liu et al., 2019; Kumar et al., 2019; Meshram et al., 2019; Nourani et al., 2019; Tao et al., 2019; Darabi et al., 2021; Üneş et al., 2021) spanning from physical-based to data-driven models as shown in Table 1 in Appendix 1.

Numerous forms of physical-based suspended sediment modeling have been proposed to cope with the unique characteristics of the sediment realm. More process-based soil loss equations include semi-empirical equations that break down the soil loss into multiple factors considering rainfall intensity, soil bulk density, soil properties, land cover and management, and soil moisture, e.g., revised universal soil loss equation (Morgan et al., 1984; Renard et al., 1991), or Morgan-Morgan-Finney (Morgan (2001)). However, one significant burden of physical-based models is that they require extensive information for development, calibration, and validation (Adnan et al., 2021) and they would first require the hydrology to be correctly simulated, which in itself has been shown recently to be suboptimal compared to machine learning models, given the information in available data (Shen 2018). Furthermore, due to the nonlinearity of sediment transport processes, calibrating the numerous parameters in such models is highly complex, requiring expert knowledge and substantial computational resources (Akay et al., 2008; Hamaamin et al., 2016; Adnan et al., 2019; Khosravi et al., 2020), and can easily run into nonuniqueness (or equifinality) issues (Beven and Rovan (2000); Beven (2006); Maren and Cronin (2016); Wu et al., 2022)).

On the other hand, data-driven models can overcome some of the drawbacks of the physical-based model. The data-driven models have demonstrated an aptitude to solve and handle modeling different hydrological variables (Afan et al., 2016; Fang and Shen (2020); Fang et al., 2020; Feng et al., 2020; Tsai et al., 2020; Ma et al., 2021; Ouyang et al., 2021; Rahmani et al., 2021; Tao et al., 2021; Tsai et al., 2021; Zhi et al., 2021; Fang et al., 2022), especially streamflow and sediment load, by capturing the non-stationarity and nonlinear behavior of SSL with fewer data than physical-based model(AlDahoul et al., 2021). However, until now, no SSC-specific data-

driven models on a large scale make universal agreements for large-scale natural resources management.

Research Objectives and Questions

This study focuses on suspended sediment concentration rather than suspended sediment flux prediction. My motivation for this work is to develop an alternative tool for predicting suspended sediment concentration on both local and continental scales over the contiguous United States (CONUS) using a state-of-the-art approach to solve challenges in measuring, calculating, and predicting the sediment concentration. This in turn can make great savings in terms of time, funding, and workforce, leading to the next step of modern paradigm for river restoration.

In this study, two types of models will be proposed: local (Local-CONUS) and continental (Whole-CONUS) scales (they will be fully described in Chapter 2, Datasets and Methodology). For the local model, it aims to delineate the trained model and explore its performance in suspended sediment concentration prediction on local scale. For continental-scale work, it aims to represent the trained sediment model on a continental scale to achieve a single model that can expand suspended sediment concentration estimates in ungauged areas (where SSC is not measured, but hydrometeorological forcing, sediment-related inputs, and streamflow information are available).

The main questions of this research are the following: (1) Can the LSTM-based models estimate the spatiotemporal SSC in the contiguous United States based on hydrometeorological forcing datasets, static watershed characteristics attributes, and streamflow with only sparse suspended concentration as the training data? (2.) Can the trained model learn to predict SSC for ungauged areas?

Chapter 2

Datasets and Methodology

Datasets

In this study, model input~~s~~ selections have been hypothesized and constructed based on a modification of the Universal Soil Loss Equation (MUSLE), an erosional model from Wischmeier and Smith (1978), suspended sediment transport mechanisms mentioned in Wohl (2020), and the past data-driven sediment models' configurations (Cigizoglu (2004); Agarwal et al., 2005; Kisi (2005); Cigizoglu and Alp (2006); Alp and Cigizoglu (2007); Lohani et al., 2007; Francke et al., 2008; Kisi (2008); Jothiprakash and Garg (2009); Rajaee et al., 2009; Firat and Gungor 2010; Melesse et al., 2011; Mustafa et al., 2012; Singh et al., 2013; Afan et al., 2014; Mustafa and Isa (2014); Olyaie et al., 2014; Kumar et al., 2016; Kaveh et al., 2017; Tasar et al., 2017; Liu et al., 2019; Kumar et al., 2019; Meshram et al., 2019; Nourani et al., 2019; Tao et al., 2019; Darabi et al., 2021; Üneş et al., 2021) to develop the most reasonable sediment model.

To cover factors that could influence sediment dynamics, the first set of inputs, which should be related to the energetic driver, are hydrometeorological forcings derived from an interpolation of a gridded meteorological dataset (Daymet) with one km by one km resolution (Thornton et al. 2016) from Google Earth Engine (GEE) (Gorelick et al. 2017) for each basin from 1980 to 2019; as a result, daily meteorological forcing data across the conterminous United States were generated (e.g., minimum and maximum temperatures, precipitation, vapor pressure, radiation, snow water equivalent, and day duration) and are shown in Table 2 in Appendix.

The second set of inputs are sediment-related static watershed features that describe the surrounding landscape and degree of regulation in the river channels. We have learned so far from studies (Yarmoshenko et al., 2020; Mahoney et al., 2018; Wohl et al., 2018; Fryirs, 2012; Borselli, 2008; Jain and Kothyari, 2000) that these features affect the sediment realm. The static watershed characteristics datasets are acquired from the Geospatial Attributes of Gages for Evaluating Streamflow dataset version II (GAGES-II), which includes geological variables, land cover, and reservoir data in 9,312 basins across the conterminous United States (Falcone 2011). A list of the watershed attributes is shown in Table 2 in Appendix. A set of non-sediment-related attributes was generated to see whether sediment-related features affect prediction performance.

The third kind of input is streamflow, as ~~in~~ most previous sediment modeling studies (Agarwal et al., 2005; Kisi, 2005; Cigizoglu and Alp (2006); Alp and Cigizoglu (2007); Lohani et al., 2007; Melesse et al., 2011; Afan et al., 2014; Goyal (2014); Mustafa and Isa (2014); Olyaie et al., 2014; Nourani and Andalib 2015; Kumar et al., 2016; Zounemat-Kermani et al., 2016; Kaveh et al., 2017; Liu et al., 2019; Kumar et al., 2019; Malik et al., 2019) included streamflow as one of the drivers of suspended sediment in river channels. It is therefore reasonable to presume that incorporating the streamflow discharge could bring additional information to our models. Although long-term records of daily streamflow discharge are available for over 23,000 US Geological Survey gaging stations in the United States, there are some sporadic missing values, so we implemented a trained LSTM-based model from Ouyang et al., 2021 (NSE = 0.71) to fill those missing values for daily streamflow observation.

The final dataset is our target SSC dataset. The USGS's National Water Information System (NWIS) database was used to download historical data for daily mean suspended sediment concentration or "SSC" (parameter code: 80154) using the public USGS-Data retrieval repository

(https://github.com/USGS-python/dataretrieval). However, data paucity of suspended sediment concentration observations limited the number of basins that could be used as inputs—only 377 sites across the contiguous United States had data both in the SSC dataset and in the static attributes from GAGES-II. The overview of information for inputs used in this study is shown in Table 1.

Table 1 Overview of inputs information

Dataset	Source	Availability
Meteorological forcing	Daymet	1980 - 2019
Static watershed attributes	Geospatial Attributes of Gages for Evaluating Streamflow dataset version II (GAGES-II)	2009
Suspended Sediment Concentration (USGS parameter code: 80154)	USGS	377 sites across the CONUS (SSC data length and distribution vary significantly from site to site)
Streamflow (USGS parameter: 00060)	USGS	1980 – 2019 (Filled missing streamflow values with Ouyang et al., 2021)

Methodology

In this study, the author chose the Long Short-Term Memory (LSTM) algorithm as the primary approach as it has gained popularity in the hydrologic and water quality realm in the last five years (e.g., Shen (2018); Fang et al., 2018; Wei et al., 2020; Rahmani et al., 2021; Rahmani et al., 2022). The LSTM approach utilizes memory cells and gates to learn and retain information over lengthy periods. Cells hold data, and gates control which data enters and exits the cells, and this memory control allows the LSTM to overcome the vanishing gradient problem faced by other algorithms (Hochreiter and Schmidhuber 1997; Fang et al., 2017, 2019). Essentially, the LSTM approach is developed to hold the gradient information over long-term memory. The overall research flow of this study is displayed in Figure 2, and the details of the LSTM will be fully described in the following sub-chapter.

The Long Short-Term Memory Architecture

Even though it sounds alien for civil engineering students, deep learning has been proved useful and can be further developed in various scientific fields. The author aims to explicitly explain the LSTM architecture mathematically as done by Lipton (2015), but simpler. The LSTM recurrent unit consists of three parts, as shown in Figure 1 The key idea is that we have the input (xt) that goes through the LSTM recurrent unit and generates the output (Ht)

The first part is called the “Forgot Gate” (forgets irrelevant information), the second part is called the “Input Gate” (adds or updates new information), and the third part is called the “Output Gate” (passes updated information). Also, the LSTM has the “Hidden State” both at the previous timestamp (Ht-1) and at the current timestamp (Ht) (the Hidden State is known as the short-term

memory), and the “Cell State” at the previous timestamp (Ct-1) and at the current timestamp (Ct) (the Cell State is known as the long-term memory, which carries the information along with all timestamps).

As the information goes along in the repeating unit, the first gate is the Forgot Gate. In this gate, it can be explained mathematically as eq. 1, where xt is an input to the current timestamp; Uf is a weight associated with the input; and Wf is the weight matrix associated with the Hidden State. A sigmoid function is then applied, so that as a result, Fgt will be a number between 0 and 1. This Fgt is then multiplied by the previous timestamp's cell state, which means how much information in the Cell State should be let through. If Fgt is 0, the network will forget everything; if Fgt is 1, it will remember everything.

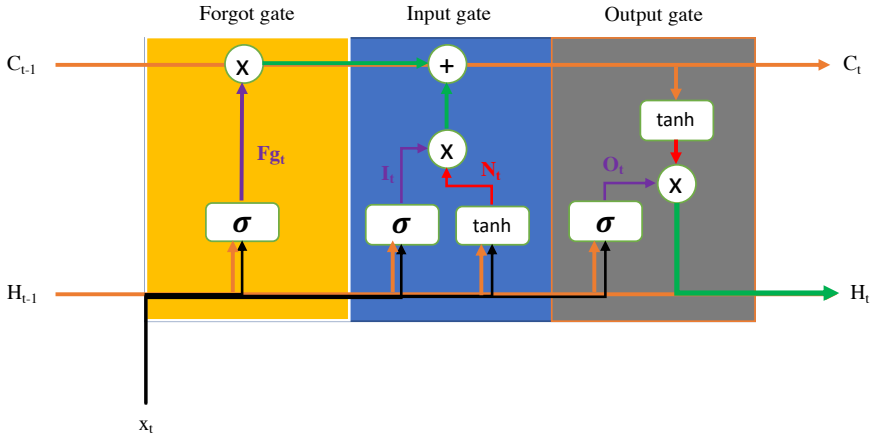

Figure 1 The LSTM repeating unit schematic flow

The next step is determining what additional information will be stored in the Cell State (the second part, the Input Gate). There are two layers in the Input Gate. The "input layer", similar to the Forgot Gate, a sigmoid layer, determines which information from the Hidden State at the previous timestamp and input at the current timestamp to update first. A “tanh layer” then generates a vector of new candidate values, Nt, that could be added to the state. The next step is to make a state update by combining eq.2 and eq. 3 as eq. 4.

Finally, the updated information in the Cell State (Ct) will move to the third part of the LSTM unit, the Output Gate. First is a sigmoid layer to determine which aspects of the cell state will be output. This sigmoid layer, again similar to the Forgot Gate, combines the previous Hidden State and the current timestamp input as eq. 5. The cell state is then passed through tanh (to force the values to be between -1 and 1) and multiplied by the output of the sigmoid gate (Ot), resulting as the Hidden State in the current timestamp, which can either be the final output we want, or can be used in the next LSTM repeating unit, and so on.

$$Fg_t = \text{sigmoid}(x_t * U_f + H_{t-1} * W_f) \quad \text{eq. 1}$$

$$I_t = \text{sigmoid}(x_t * U_i + H_{t-1} * W_i) \quad \text{eq. 2}$$

$$N_t = \tanh(xt * U_N + H_{t-1} * W_N) \quad \text{eq. 3}$$

$$C_t = Fg_t * C_{t-1} + I_t * N_t \quad \text{eq. 4}$$

$$O_t = \text{sigmoid}(x_t * U_o + H_{t-1} * W_o) \quad \text{eq. 5}$$

$$H_t = O_t * \tanh(C_t) \quad \text{eq. 6}$$

Local-CONUS and Whole-CONUS approaches

The author implemented two training-and-testing approaches to answer the research questions in this study.

The first approach is called the "Local-CONUS" or "local", in which a model is trained and tested locally for each of the 377 basins in the compiled dataset. At the end, 377 LSTM-based models will be generated). The schematic flow of research is portrayed in Figure 2 (left, blue).

The second approach is called the Whole-CONUS model. This approach will randomly select data points from a 377-basin training data pool to train the model, then test the trained model with a different date-time range for each site. At the end, one single LSTM-based model will be generated), as shown in Figure 2 (right, green).

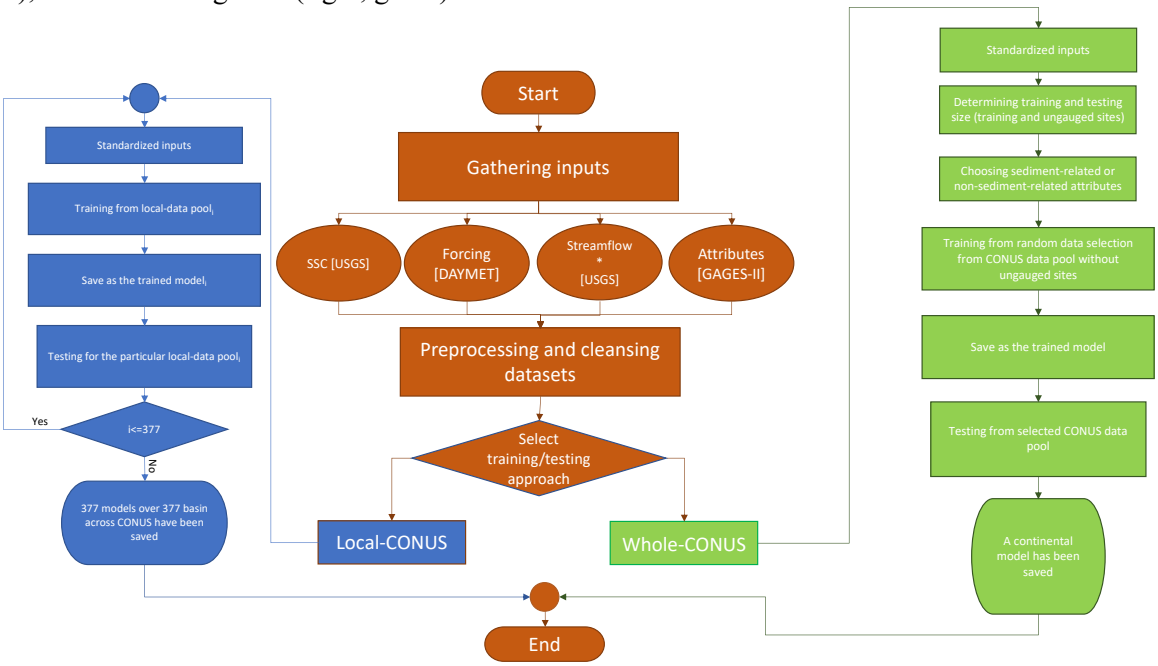

Figure 2 Schematic flow of research

Preprocessing steps

Reliability of Suspended Sediment sampling to Suspended Sediment Concentration datasets

The suspended sediment concentration raw datasets have been retrieved from the National Water Information system, USGS. The USGS studies (U.S. Geological Survey, 1997; Wilde and others, 1999; Gray et al., 2000) showed that the accuracy of churn splitter and cone splitter subsamples is considered inadequate at SSC values of 10,000 mg/L or above. Thus, in this study, we set the ceiling of the suspended sediment concentration to 10,000 mg/L (1.65% of available suspended sediment concentration data are more than 10,000 mg/L).

Standardizations and De-standardizations

The inputs were standardized before being fed to training processes. The standardization procedures compel a trained model to pay equal attention to large wet and small dry basins (Feng et al., 2020; Rahmani et al., 2021; Wenyu et al., 2021). Firstly, we created a dimensionless streamflow distribution by partitioning both basin area and mean annual precipitation in the particular basin. Then we transformed dimensionless streamflow into a new, more Gaussian distribution as eq. 7 (Feng et al., 2020; Wenyu et al., 2021; Rahmani et al., 2022). Note that 0.1 is the constant included to cope with any zero values of the streamflow. We also applied log-transformation eq. 8 to suspended sediment concentration datasets to minimize the skewness of the broad range of SSC values (spanning from 0.1 to 10,000) based on the common assumption that the suspended sediment concentration is log-normally distributed (Holtschlag 2001).

$$f^* = \log_{10}(\sqrt{f} + 0.1) \qquad \text{eq. 7}$$

$$f^* = \log_{10}(\sqrt{f}) \qquad \text{eq. 8}$$

Where f^* and f are transformed streamflow and observed raw streamflow, respectively. Next, we standardized all forcings, static attributes, transformed streamflow, and SSC observations by the eq. 9

$$x_{new,i} = \frac{(x_i - \bar{x})}{\sigma} \qquad \text{eq. 9}$$

Where $x_{new,i}$ is the standardized values, x_i is the raw observed value, $\bar{x}$ is the variable's mean, and σ is the variable's standard deviation. In the end, all output from the model will be de-standardized before statistical metrics calculations.

Loss function and statistical metrics for model evaluations

Root-mean-square error(RMSE)

Root-mean-square error (RMSE) was applied as the loss function for each model. RMSE is defined as the square root of the mean of the square of all errors. The RMSE error metric is widely used and is regarded as an excellent general-purpose error measure for numerical forecasts. The RMSE can be calculated as in eq. 10:

$$\text{RMSE} = \sqrt{\sum_i^n \frac{(pred_i - obs_i)^2}{n}} \qquad \text{eq. 10}$$

Bias

Bias is the gap between the estimated and actual values, which can be calculated as the eq. 11:

$$\text{Bias} = \sum_i^n (pred_i - obs_i) \qquad \text{eq. 11}$$

Unbiased-Root Mean Squared (ubRMSE)

From the metrics mentioned above, we can calculate the unbiased root-mean-square error by subtracting the mean bias from the mean root-mean-square error.

Nash-Sutcliffe coefficient (NSE)

The Nash–Sutcliffe model efficiency coefficient (NSE) is used to evaluate hydrological models' forecasting ability (Nash and Sutcliffe 1970). NSE ranges from 0 to 1, with 1 indicating a perfect match between model prediction and observation. However, NSE 0 implies poor performance, with model prediction poorer than mean observations. It is defined as follows in eq. 12:

$$NSE = 1 - \frac{\sum_i^n (pred_i - obs_i)^2}{\sum_i^n (obs_i - \overline{obs})^2} \qquad \text{eq. 12}$$

Moriasi et al., 2015 considered performance measures and evaluation criteria regarding physical-based hydrologic and water quality models to predict suspended sediment concentration on a monthly temporal scale and a watershed-scale spatial scale, and concluded that Very Good NSE is more than 0.80, Good NSE is in between 0.70 and 0.80, Satisfactory NSE is in between 0.45 and 0.70, and Unsatisfactory NSE is lower than 0.45. Moriasi also mentioned that lacking observations and difficulties of model calibration, model validation, model initializations, etc. in physical-based modeling limited the final performance criteria to a monthly scale and to watershed and local scales.

Pearson's correlation coefficient (R)

Pearson's correlation coefficient measures the linear correlation between two sets of data (predictions and observations). The Pearson's values range from -1 to 1 for the perfect negative and positive correlation. It is defined as eq. 13:

$$R = \frac{\sum_i^n (pred_i - \overline{pred_i})(obs_i - \overline{obs_i})}{\sqrt{\sum_i^n (pred_i - \overline{pred_i})^2 \sum_i^n (obs_i - \overline{obs_i})^2}} \qquad \text{eq. 13}$$

The Coefficient of determination (R^2)

R^2, a coefficient of determination, is used to determine how differences in one variable may be explained by variations in another. Typically, the coefficient of determination ranges from 0 to 1. It can be calculated as eq. 14:

$$R^2 = \frac{n\sum_i^n (pred_i \times obs_i) - \sum_i^n (pred_i) \sum_i^n (obs_i)}{\sqrt{n[\sum_i^n (pred_i)^2 - (\sum_i^n pred_i)^2] n[\sum_i^n (obs_i)^2 - (\sum_i^n obs_i)^2]}} \qquad \text{eq. 14}$$

Hyperparameter, training and testing

Hyperparameters

In the realm of Deep Learning, hyperparameters are characteristics of the deep learning model itself, which influence the learning process and affect the model performance. The first hyperparameter is the number of epochs used, which refers to the number of rounds through the full training dataset that the training has completed. The second hyperparameter is Rho or "ρ" which is a constant time window used in sampling time-series datasets (hydrometeorological forcings and suspended sediment concentration, our target) in the training process. The unit of rho is days. The third hyperparameter, batch size, is the number of training samples used in one iteration. The fourth

is the hidden size, or the number of hidden layers in the neural network. And the last one, dropout, indicates the percentage of generalization during the training process to cope with overfitting issues. During training, some layer outputs are disregarded or "dropped out" at random. In this case, Dropout is equal to 0.5, meaning that 50% of data in one iteration is dropped out.

However, this study has not concluded optimized investigations as it focuses on addressing the accuracy and insights between local and continental scales. As such, the same hyperparameters were utilized in Local-CONUS and Whole-CONUS, and are listed in Table 2.

Table 2 Hyperparameters for Local-CONUS, Whole-CONUS (all sites), and Whole-CONUS (ungauged experiment)

Model/Hyperparameters	*Epochs*	*Rho*	*Hiddensize*	*Batchsize*	*Dropout*
Local-CONUS	*100*	*30*	*100*	*40*	*0.5*
Whole-CONUS with all sites	*100*	*30*	*256*	*40*	*0.5*
Whole-CONUS (ungauged experiment)	*300*	*365*	*200*	*40*	*0.5*

Training and Testing

Due to data availability, data length, and distribution of suspended sediment concentration varying from site to site as shown in Figure 3, the traditional constant time window for training and testing of the LSTM-based model as done in previous studies (Rahmani et al., 2021; Zhi et al., 2021; Ouyang et al., 2021; Fang et al., 2020) may exclude some sites that may hold data points in training but do not hold data points in testing, or conversely, hold in testing but do not hold in training. Furthermore, to optimize all existing observations in such a scarce suspended sediment concentration dataset, the Maximum Sub-Array Sum algorithm (Takaoka (2002)) was implemented to find the proper training and testing periods for each site, which are listed in Appendix-Table 5 DNP. The author called this method of training and testing the “DNP” (e.g., Days and Periods). The process of DNP is simple. In a training process, a random starting date (e.g., nt in train.py) for sampling data from the data pool is generated solely in the range of the DNP in each site (e.g., ngrid in train.py), and in the testing process, all the other observations outside of the testing period in DNP will turn up in np.nan. This means we will test the predicted data with the observation in the testing period from the DNP.

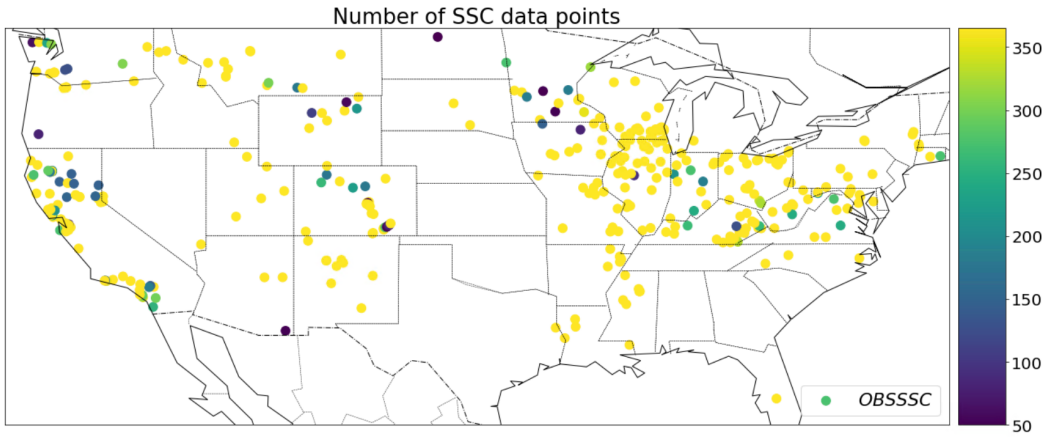

Figure 3 Number of SSC data points for each site across the Contiguous United State

Chapter 3

Results

In this chapter, results from analyses are provided in 3 main sections: (1) Raw datasets analysis; (2); The local model results; (3) The Whole-CONUS results, which comprise two subsections (all-site predictions and ungauged stations predictions).

Raw datasets analysis

In this section, the maps of SSC observation, hydrometeorological forcings, and a selected attribute (e.g., hydrological disturbance index) are plotted to demonstrate the spatial variability and range. Only one static watershed attribute, the hydrological disturbance index, is plotted. This parameter is dimensionless and significantly impacts sediment regimes (details about this parameter are in Table 2 in Appendix). The day length variable was not plotted, since it does not significantly vary from site to site. However, it was still included as an input for the model.

The distribution maps of the daily value of variables for each site are shown in Figure 1 to Figure 13 below, with the color bar indicating the degree of importance. The Mountain West region of the CONUS (as the Rocky Range) shows a relatively high value of suspended sediment concentration, and relatively low values of SSC are seen in the Mid Atlantic and near-coast area (the 5th and 85th percentiles of the average suspended sediment concentration are 7.19 and 309.78 [mg/L], respectively). SSC is higher in the western basins where rainfall is decidedly lower, suggesting that vegetative protection plays an important role in preventing soil erosion.

The average daily shortwave radiation shows a significantly high value in the South-West region of the CONUS, and for other regions, the higher average value of the radiation moves to the lower value longitudinally (the 5th and 85th percentiles of the shortwave radiation are 297.00 and 388.35 [W/m2], respectively). The average daily precipitation is significantly high in the Northeastern and Eastern regions and relatively low in the Southwest of the CONUS (the 5th and 85th percentiles of the shortwave radiation are 1.06 and 3.82 [mm/day], respectively). The maximum and minimum air temperatures have a similar variation which is relatively higher in the northern region and lower in the southern region. The 5th and 85th percentiles of the average daily maximum air temperature are 10.84 and 20.18 [degrees Celsius], respectively. The 5th and 85th percentiles of the average daily air minimum temperature are -2.41 and 7.68 [degrees Celsius], respectively. The water vapor pressure is relatively high in the southern region (the 5th and 85th percentiles of the vapor pressure are 474.38 and 1121.20 [Pa], respectively). The snow water equivalent is relatively high in the north of the CONUS (the 5th and 85th percentiles of the vapor pressure are 0.0012 and 32.18 [kg/m2]). For streamflow, it makes sense that the spatial variation of the streamflow is irregular because the flow regimes are interrupted by regulations, fragmentations, and anthropogenic modifications. The 5th and 85th percentiles of the streamflow are 3.56 and 2075.27 [ft3/s]. Similarly, for the selected attribute, the hydrological disturbance index scatters with no clear continental-scale patterns (the 5th and 85th percentiles are 1 and 20 [ft3/s].

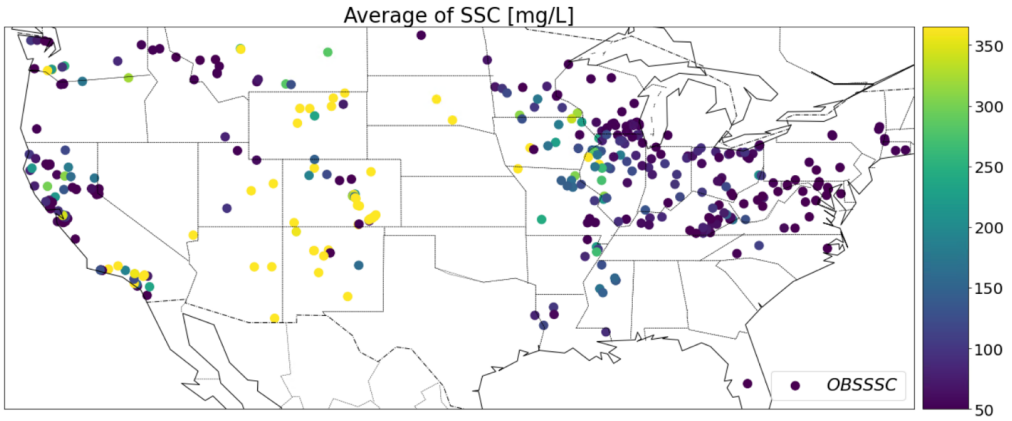

Figure 4 Average Daily Suspended Sediment Concentration of each site across the CONUS [mg/L]

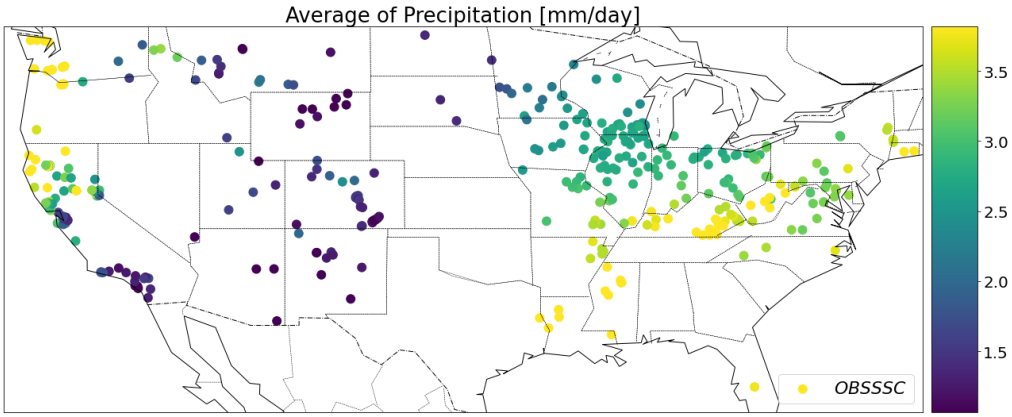

Figure 5 Average Daily Precipitation of each site across the CONUS [mm/day]

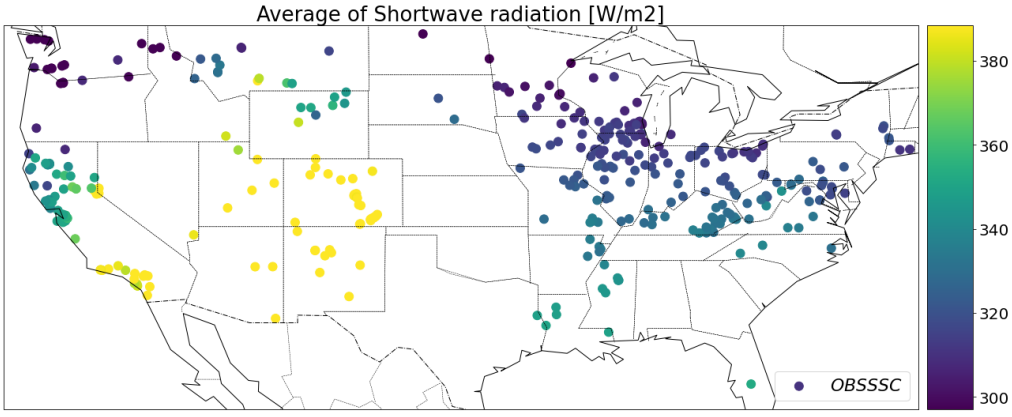

Figure 6 Average Daily Shortwave Radiation of each site across the CONUS [W/m2]

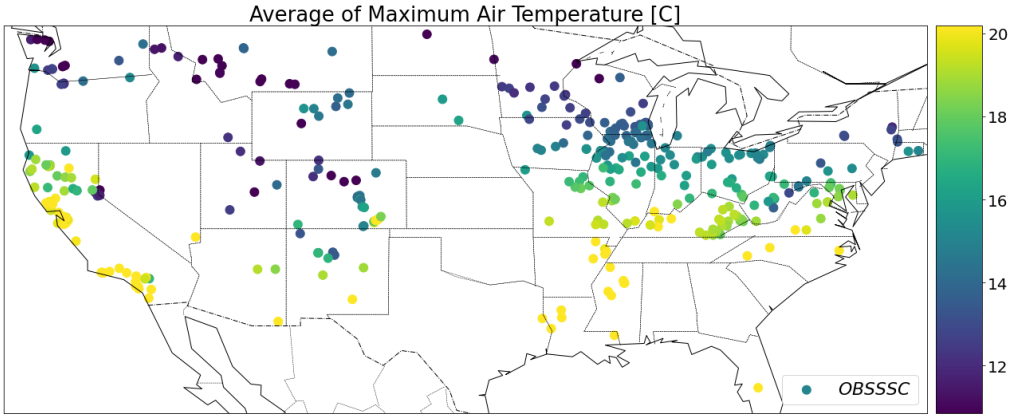

Figure 7 Average Daily Maximum Air Temperature of each site across the CONUS [C]

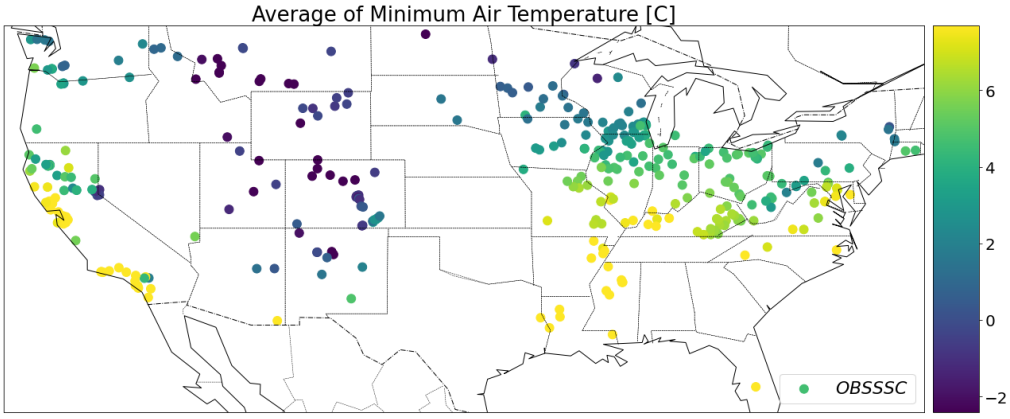

Figure 8 Average Daily Minimum Air Temperature of each site across the CONUS [C]

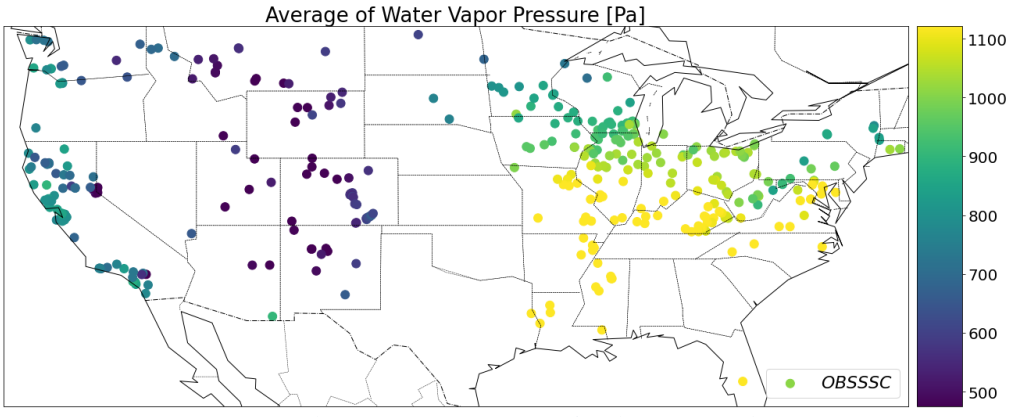

Figure 9 Average Daily Water Vapor Pressure of each site across the CONUS [Pa]

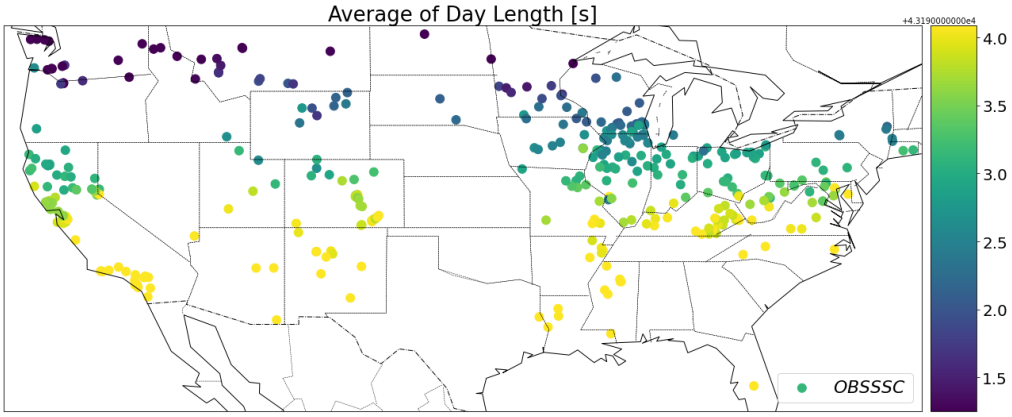

Figure 10 Average Daily Day Length of each site across the CONUS [second]

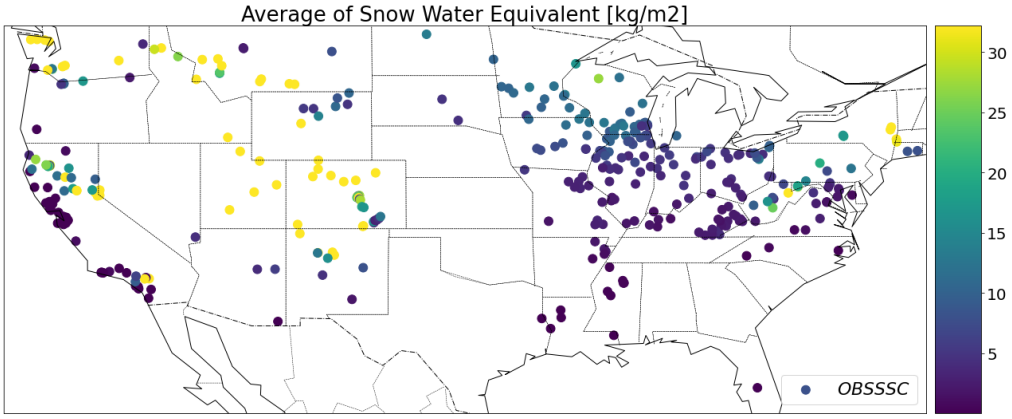

Figure 11 Average Daily Snow Water Equivalent of each site across the CONUS [Kg/m2]

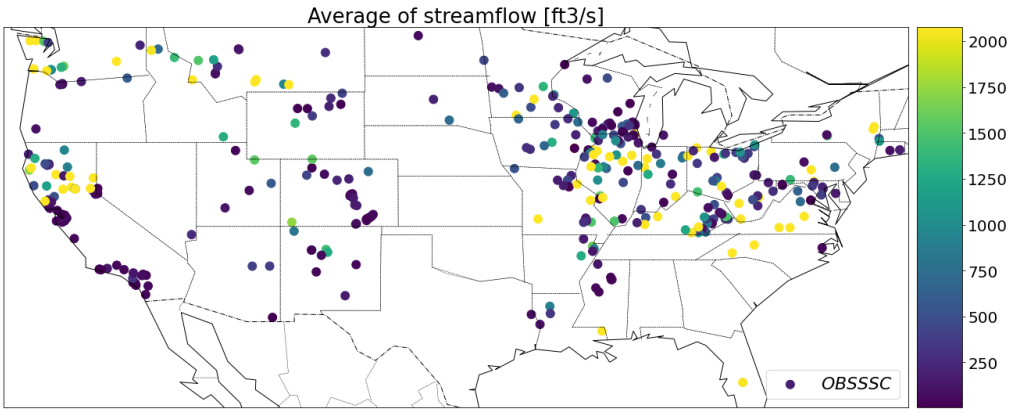

Figure 12 Average Streamflow of each site across the CONUS [ft/s]

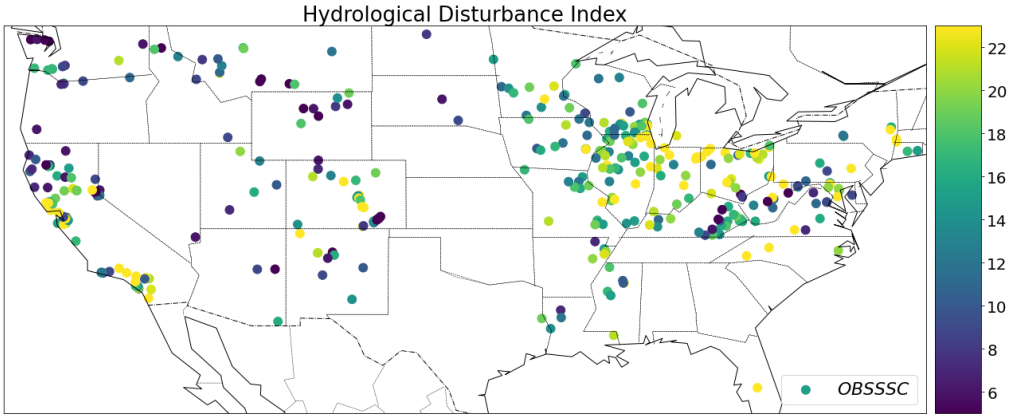

Figure 13 Hydrological Disturbance Index of each site across the CONUS

Results from the Local-CONUS approach

377 local models were trained; one for each basin with sufficient data. The models were trained and tested individually with sediment-related attributes. In the end, the 377 models' training and testing performances across the contiguous United States were plotted as box plots, which are shown below in Figure 14 and Figure 15. The horizontal line in each box represents the median and the bottom and top of the box represent the first and third quantiles, respectively, while the whiskers represent the minimum and maximum values, respectively. Further, the local models presented exceptional median metrics as provided in Table 3.

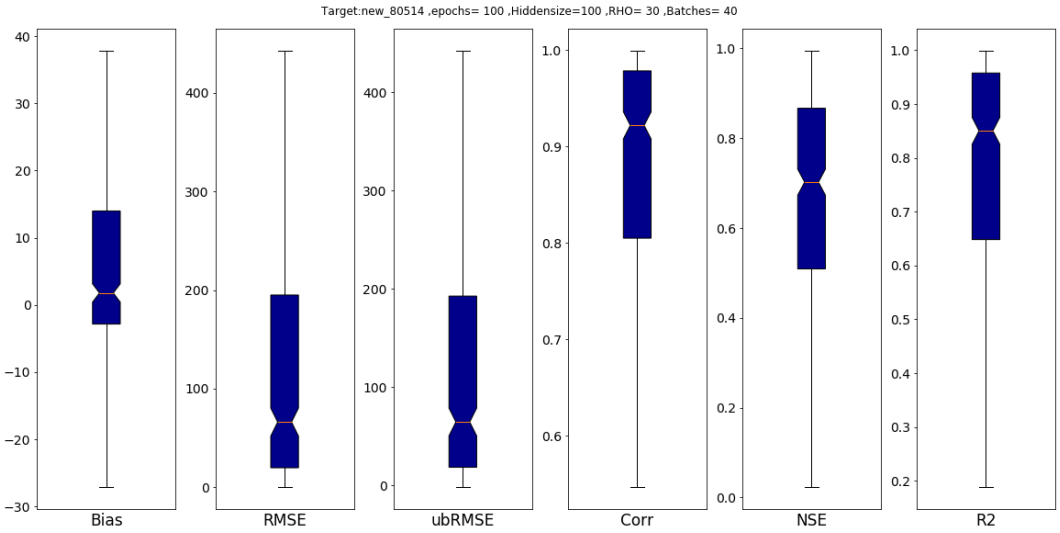

Figure 14 The Local-CONUS box plot of statistical metrics in training

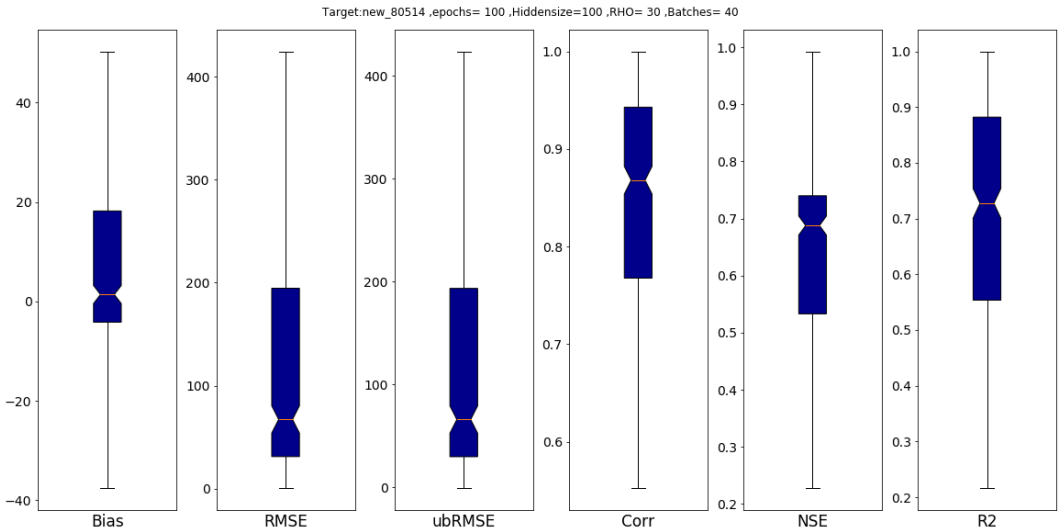

Figure 15 The Local-CONUS box plot of statistical metrics in testing

Table 3 Statistical metrics of all Local-CONUS models with sediment-related attributes

Statistical Metric	median value (Training)	median value (Testing)
Bias [mg/L]	1.781	1.379
RMSE [mg/L]	66.156	67.295
Unbiased RMSE [mg/L]	64.740	65.834
Pearson's Correlation (R)	0.922	0.868
Nash-Sutcliff Efficiency	0.702	0.687
Coefficient of determination (R^2)	0.850	0.727

Results from the Whole-CONUS approach

All-Site Predictions Experiment with sediment-related attributes

In this experiment, the Whole-CONUS model has been developed as a trained and tested model from a 377-station data pool. The model generates estimated SSC values, which are then compared with the actual values measured at the 377 stations. In the end, the Whole-CONUS model's training and testing performance across the contiguous United States has been plotted as box plots, which are shown below in Figure 16 and Figure 17. The horizontal line in each box represents the median and the bottom and top of the box represent the first and third quantiles, respectively, while the whiskers represent the minimum and maximum values, respectively. The median statistical metrics of training and testing are also provided in Table 4.

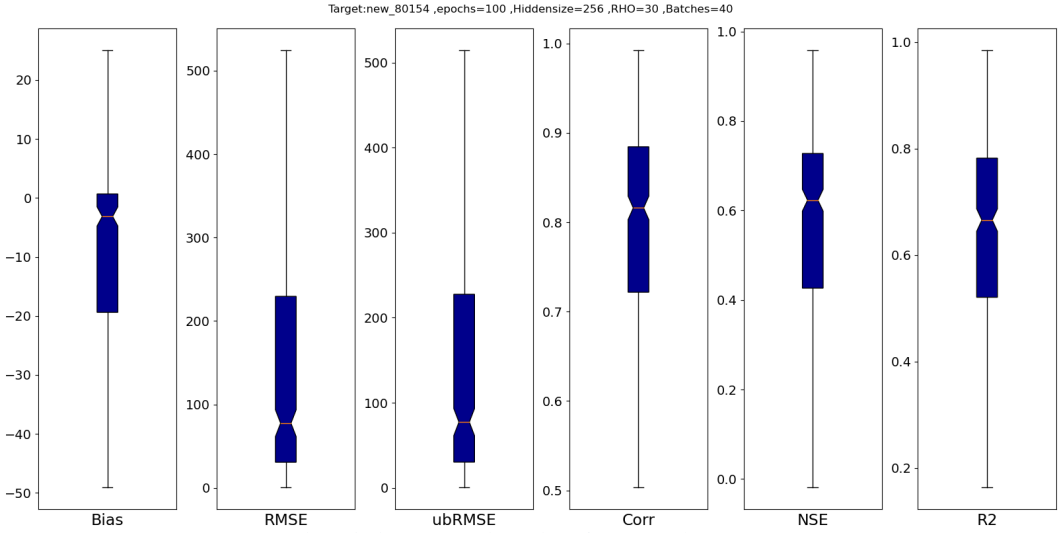

Figure 16 The Whole-CONUS box plot of statistical metrics in training

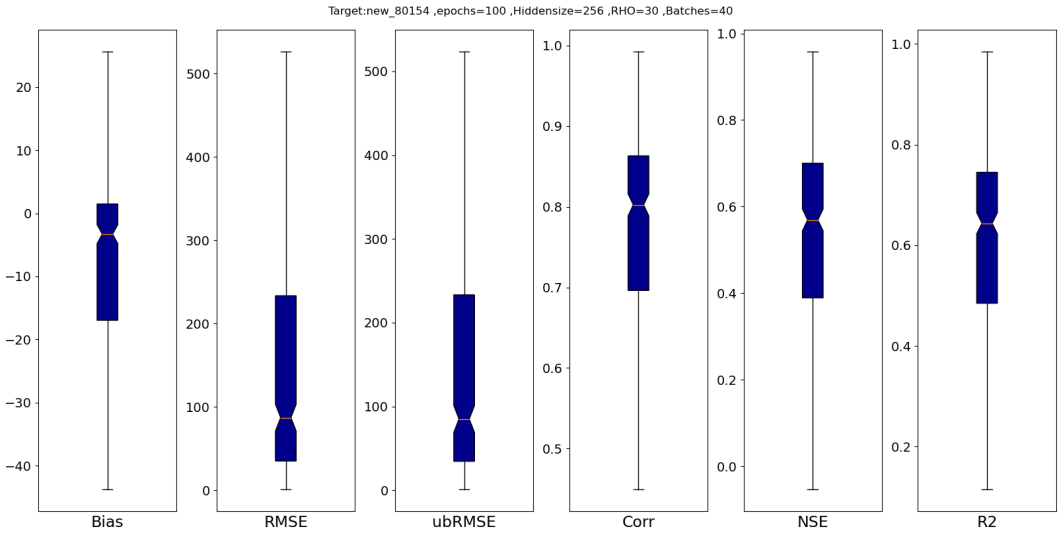

Figure 17 The Whole-CONUS box plot of statistical metrics in testing

Table 4 Statistical metrics of Whole-CONUS model with sediment-related attributes

Statistical Metric	median value (Training)	median value (Testing)
Bias [mg/L]	-3.138	-3.403
RMSE [mg/L]	77.471	79.303
Unbiased RMSE [mg/L]	77.255	78.978
Pearson's Correlation (R)	0.816	0.806
Nash-Sutcliff Efficiency	0.621	0.596
Coefficient of determination (R^2)	0.665	0.645

All-Site Predictions Experiment with non-sediment-related attributes

With the same configuration as above, the Whole-CONUS model with random vectors has been developed as a trained and tested model from a 377-station data pool, but was trained using non-sediment-related attributes (random vectors), as some argued that deep learning models are

powerful enough to memorize random vectors for site characterization (Li et al., 2022). In the end, the Whole-CONUS model's training and testing performance across the contiguous United States was plotted as box plots, shown below in Figure 16 and Figure 17. The horizontal line in each box represents the median and the bottom and top of the box represent the first and third quantiles, respectively, while the whiskers represent the minimum and maximum values, respectively. The median statistical metrics of training and testing are also provided in Table 4.

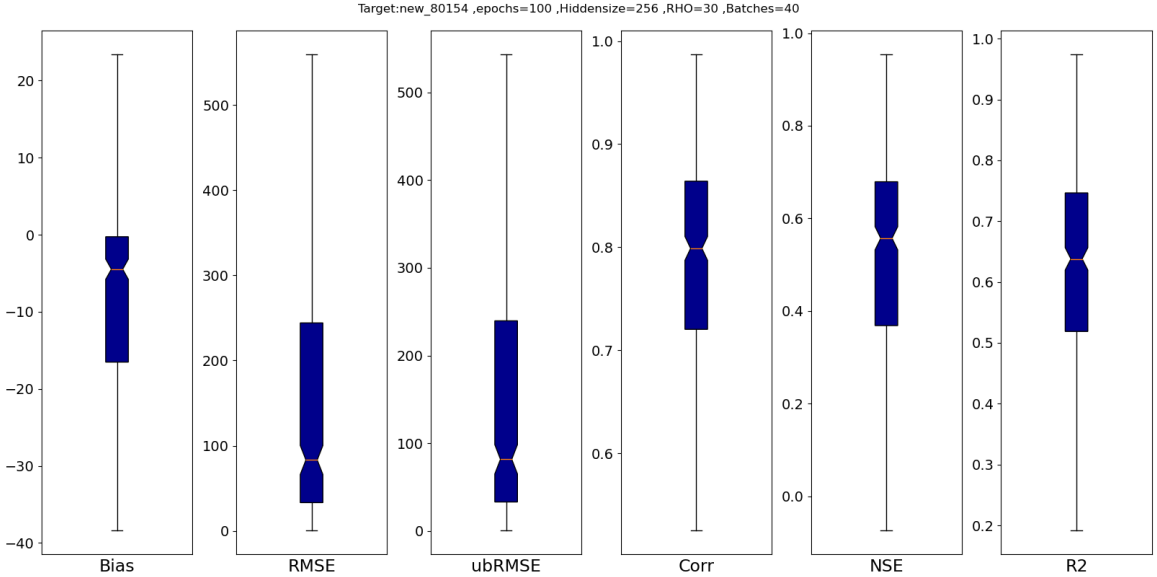

Figure 18 The Whole-CONUS box plot of statistical metrics in training with non-sediment-related attributes

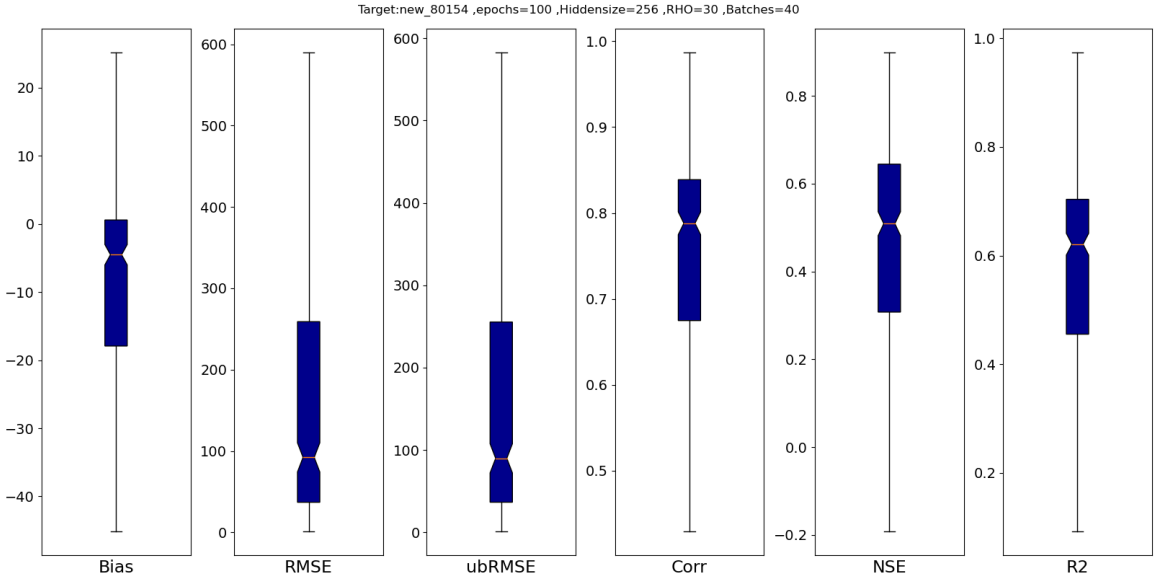

Figure 19 The Whole-CONUS box plot of statistical metrics in testing with non-sediment-related attributes

Table 5 Statistical metrics of all Whole-CONUS model with non-sediment-related attributes

Statistical Metric	median value (Training)	median value (Testing)
Bias [mg/L]	-4.476	-4.507
RMSE [mg/L]	83.254	92.186
Unbiased RMSE [mg/L]	81.621	89.826
Pearson's Correlation (R)	0.798	0.788
Nash-Sutcliff Efficiency	0.557	0.508
Coefficient of determination (R^2)	0.638	0.621

The Ungauged Prediction Experiment

In this experiment, the Whole-CONUS model was built up from a 284-basin data pool and tested with a 93-basin data pool (instead of training and testing from the entire 377-basin data pool) to see its capability to overcome ungauged areas. The 93 ungauged stations were split with simple criteria: the number of raw data should be more than 365. And the reason that came up with the criteria is the model can be tuned with hyperparameter rho equal to 365 for reducing computational time (it runs faster with hyperparameter rho = 365). The box plots for the 284-basin model and ungauged station performance are shown in Figure 20, Figure 21, and Figure 22, respectively, and median metrics of the ungauged performance are listed in Table 6.

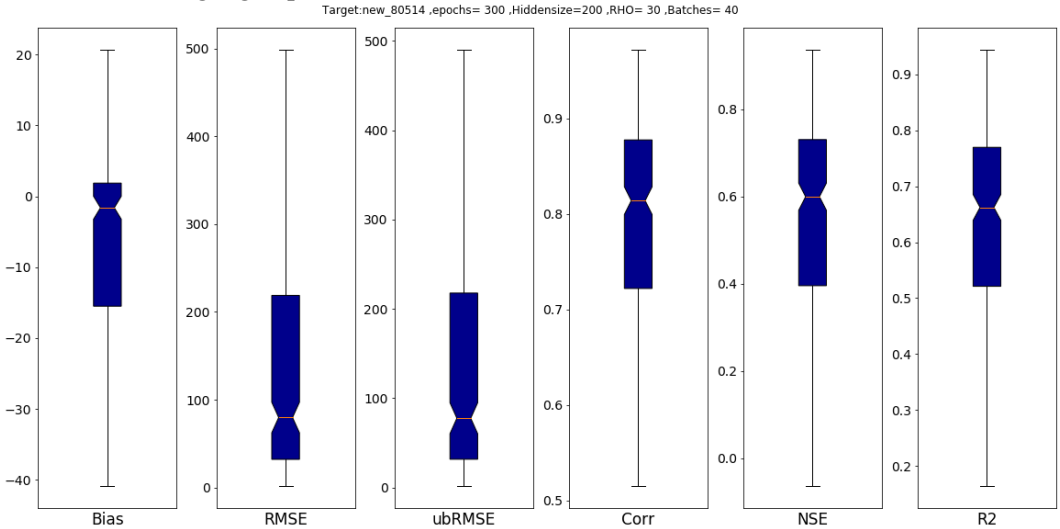

Figure 20 The Whole-CONUS box plot of statistical metrics in 284-stations training

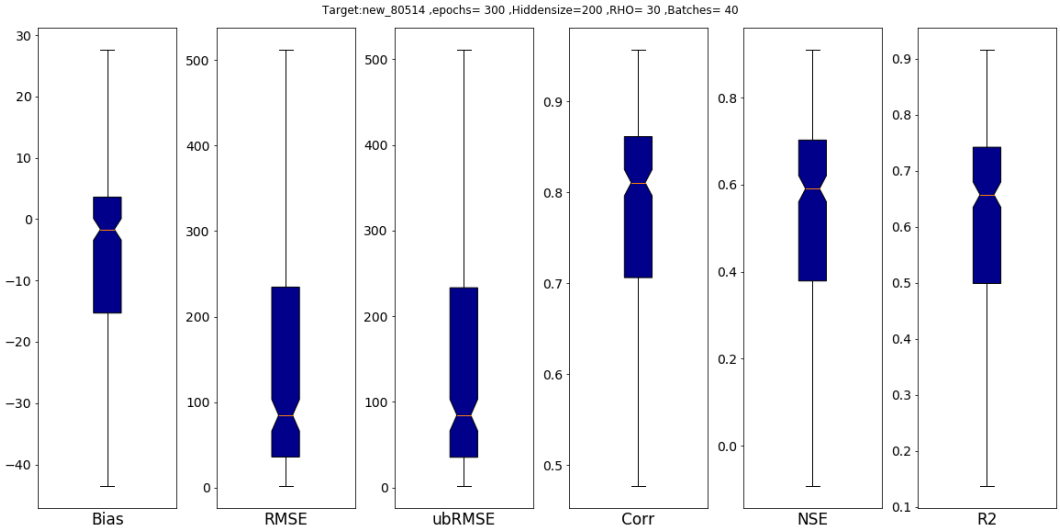

Figure 21 The Whole-CONUS box plot of statistical metrics in 284-stations testing

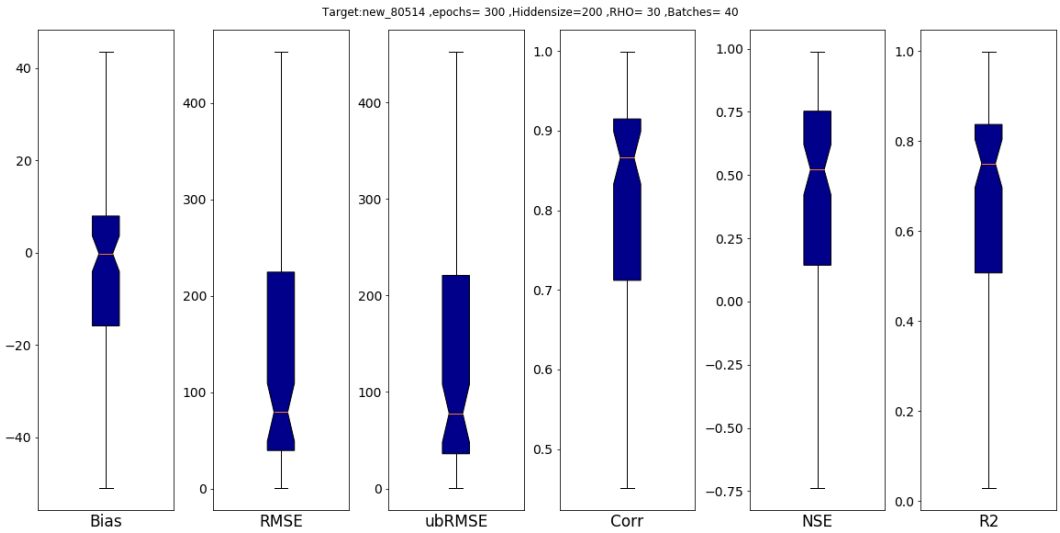

Figure 22 The Whole-CONUS box plot of statistical metrics in 93-stations testing

Table 6 Statistical metrics of the Whole-CONUS model in The Ungauged Prediction Experiment

Statistical Metric	median value (284-station training)	median value (284-station testing)	Median value (Ungauged stations testing)
Bias [mg/L]	-1.619	-1.669	-0.211
RMSE [mg/L]	79.758	84.598	79.129
Unbiased RMSE [mg/L]	77.507	84.573	77.868
Pearson's Correlation (R)	0.813	0.810	0.865
Nash-Sutcliff Efficiency	0.599	0.591	0.521
Coefficient of determination (R^2)	0.662	0.657	0.749

Chapter 4

Discussion

The 1st Research question: Can the LSTM-based model predict the suspended sediment concentration across the contiguous United States from intensive hydrometeorological forcing, static watershed attributes, streamflow, and sparse suspended sediment concentration?

As discussed in Chapter 2, this study will follow the criteria from Moriasi et al., 2015. For the Local-CONUS approach in a training session, there are 75 sites with an NSE < 0.45 (approximately 20 percent of the available 377 sites), 107 sites with 0.45 < an NSE < 0.7 (approximately 29 percent), 49 sites with 0.70 < an NSE ≦ 0.8 (approximately 13 percent), and 146 sites with an NSE > 0.8 (approximately 38 percent). For the Local-CONUS approach in a testing session, there are 54 sites with an NSE < 0.45 (approximately 14 percent of available sites), 164 sites with 0.45 < an NSE < 0.7 (approximately 44 percent), 89 sites with 0.70 < an NSE ≦ 0.8 (approximately 23 percent), and 70 sites with an NSE > 0.8 (approximately 19 percent).

For the Whole-CONUS approach with all sites (377 sites) in a training session, there are 102 sites with an NSE < 0.45 (approximately 27 percent of available sites), 155 sites with 0.45 < an NSE < 0.7 (approximately 41 percent), 70 sites with 0.70 < an NSE ≦ 0.8 (approximately 19 percent), and 50 sites with an NSE > 0.8 (approximately 13 percent). For the Whole-CONUS approach with all sites in a testing session, there are 124 sites with an NSE < 0.45 (approximately 32 percent of available sites), 158 sites with 0.45 < an NSE < 0.7 (approximately 42 percent), 62 sites with 0.70 < an NSE ≦ 0.8 (approximately 17 percent), and 33 sites with an NSE > 0.8 (approximately 9 percent). These results are summarized in Table 7.

The author expects to see a higher error of prediction in the system on different scales (higher RMSE, lower NSE, and lower R2, to name a few) as previous studies in water quality as such dissolved oxygen prediction showed that the higher the spatial scale, the higher the RMSE error (Hu et al., 2019). Likewise, the higher temporal scale is expected to show a lower RMSE, as Aldahoul et al., 2021 showed that daily scale suspended sediment concentration prediction results hold a higher RMSE error than weekly and monthly results.

Cohen et al., 2013 showed an average of 0.29 Coefficient of Determination of suspended sediment concentration over 11 sites across the CONUS, which is far below the median coefficient of the LSTM-based model reported here, equal to 0.86 and 0.67 for Local-CONUS and Whole-CONUS approaches, respectively, even though the Local-CONUS and the Whole-CONUS models are on a larger spatial scale.

The differences in performance between the Local-CONUS and Whole-CONUS approaches imply that the continental scale prediction is more complex compared to the local scale prediction, even though the number of hidden layers of the Local-CONUS is lower than the Whole-CONUS in terms of the model structure. The differences also lead the author to question the current set of attributes and how crucial the current attributes are. Considering results from the Whole-CONUS models that have been trained with sediment-related and non-sediment-related attributes with the same configurations as shown in Figure 24, they confirm the importance of the sediment-

related attributes: the attributes do provide knowledge and information helping the model capture suspended sediment concentration characteristics in river channels. Thus, it can be implied that the current set of static watershed descriptors inputs still lacks critical information regarding certain processes that are highly relevant to suspended sediment production. The LSTM-based model may need new inputs, e.g., management practices, stream channel width distributions, etc.

Juez et al., 2018 and Tao et al., 2021 also mentioned that processes of the riverbed modulate the hysteresis behaviors of suspended sediment in different rivers, and adequately modeling suspended sediment needs new strategies considering the inputs, including the morphological changes in the riverbed. Unfortunately, this study does not include any information about riverbed or riverbed grain size changes. The missing riverbed descriptor may contribute to the reason that the Whole-CONUS model did not perform as well as the Local-CONUS approach.

Figure 25 reflects that the model will fail to capture the dynamics of SSC if there are significant broad differences in the magnitude of SSC observations between the training and the testing periods. The author expects that these differences come from external factors that control observed data qualities, such as illegal dumping, dredging, or other events that act as “hot spots” and “hot moments” and make the suspended sediment concentration abruptly increase in a short time. Thus, it can be implied that the models will effectively capture the suspended sediment dynamic when those sites are less disruptive (no external factors, hot spots, or hot moments) or have fewer differences observations used for training and testing.

To conclude, results from this study clearly show that LSTM-based models can predict suspended sediment concentration from rich-data hydrometeorological forcing, sediment-related static watershed attributes, and streamflow data with overall satisfying performance in both approaches across the contiguous United States as portrayed in Figure 14 to Figure 21. The author argues that the strength of the approaches is that the models include watershed features such as land use and land cover, stream density, soil properties, geological parameters, and anthropogenic modifications like the presence of dams, etc., which are difficult to calibrate and include in traditional models. The models only require the hydrometeorological forcings, sediment-related static watershed attributes, and streamflow data which are much more available datasets compared to suspended sediment concentration. If the datasets above are available, the best way to predict SSC in the river channel is to train the model as the Local-CONUS models shown in this work.

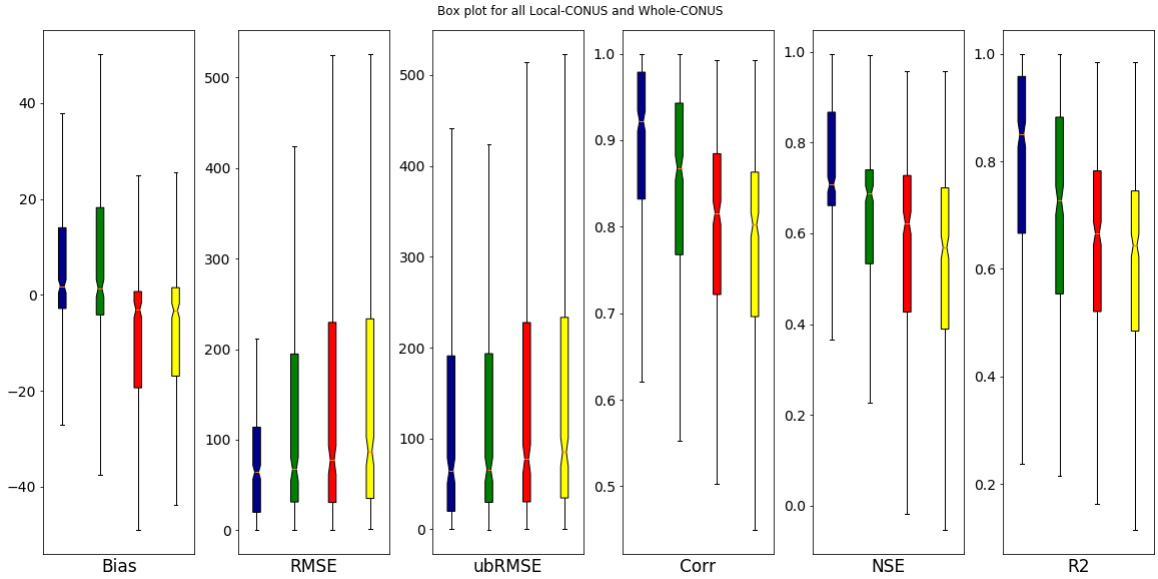

Figure 23 Statistical metric plots for Local-CONUS and Whole-CONUS (Blue is the Local-CONUS in a training session; Green is the Local-CONUS in a testing session; Red is the Whole-CONUS in a training session; Yellow is the Whole-CONUS in a testing session

Table 7 Number of sites' performance distributed in each criterion

Model/session	NSE < 0.45 (Unsatisfactory)	0.45< NSE ≦ 0.7 (Satisfactory)	0.7 < NSE 0.8 (Good)	NSE > 0.8 (Very good)
Local-CONUS/ Training	76	110	54	137
Local-CONUS/ Testing	86	109	119	63
Whole-CONUS with all sites /Training	102	155	70	50
Whole-CONUS with all sites /Testing	124	158	62	33

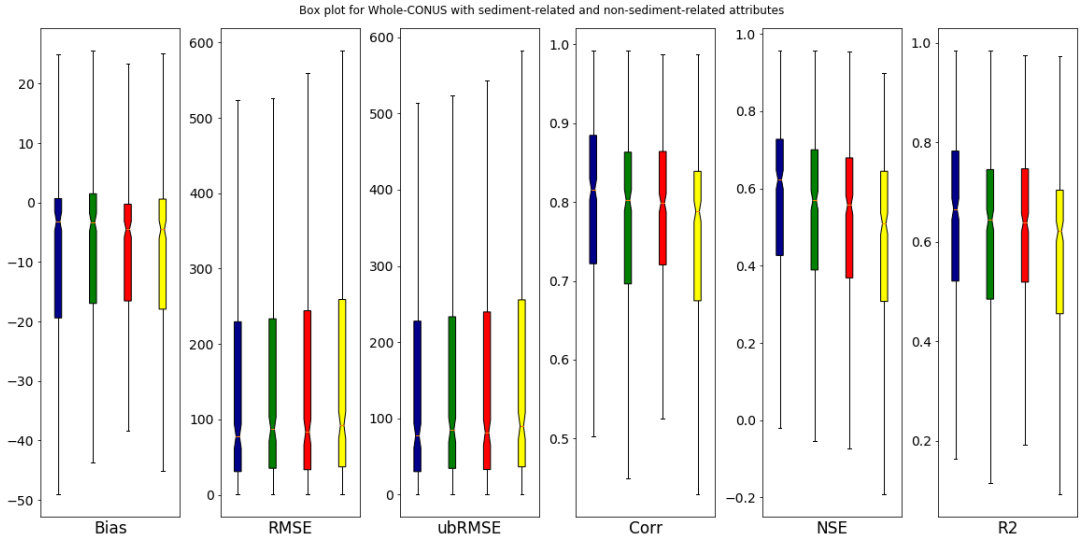

Figure 24 Statistical metric plots for Whole-CONUS with sediment-related and non-sediment-related attributes (Blue is the Whole-CONUS with sediment-related attributes in a training session; Green is the Whole-CONUS with sediment-related attributes in a testing session; Red is the Whole-CONUS with non-sediment-related attributes in a training session; Yellow is the Whole-CONUS with non-sediment-related attributes in a testing session

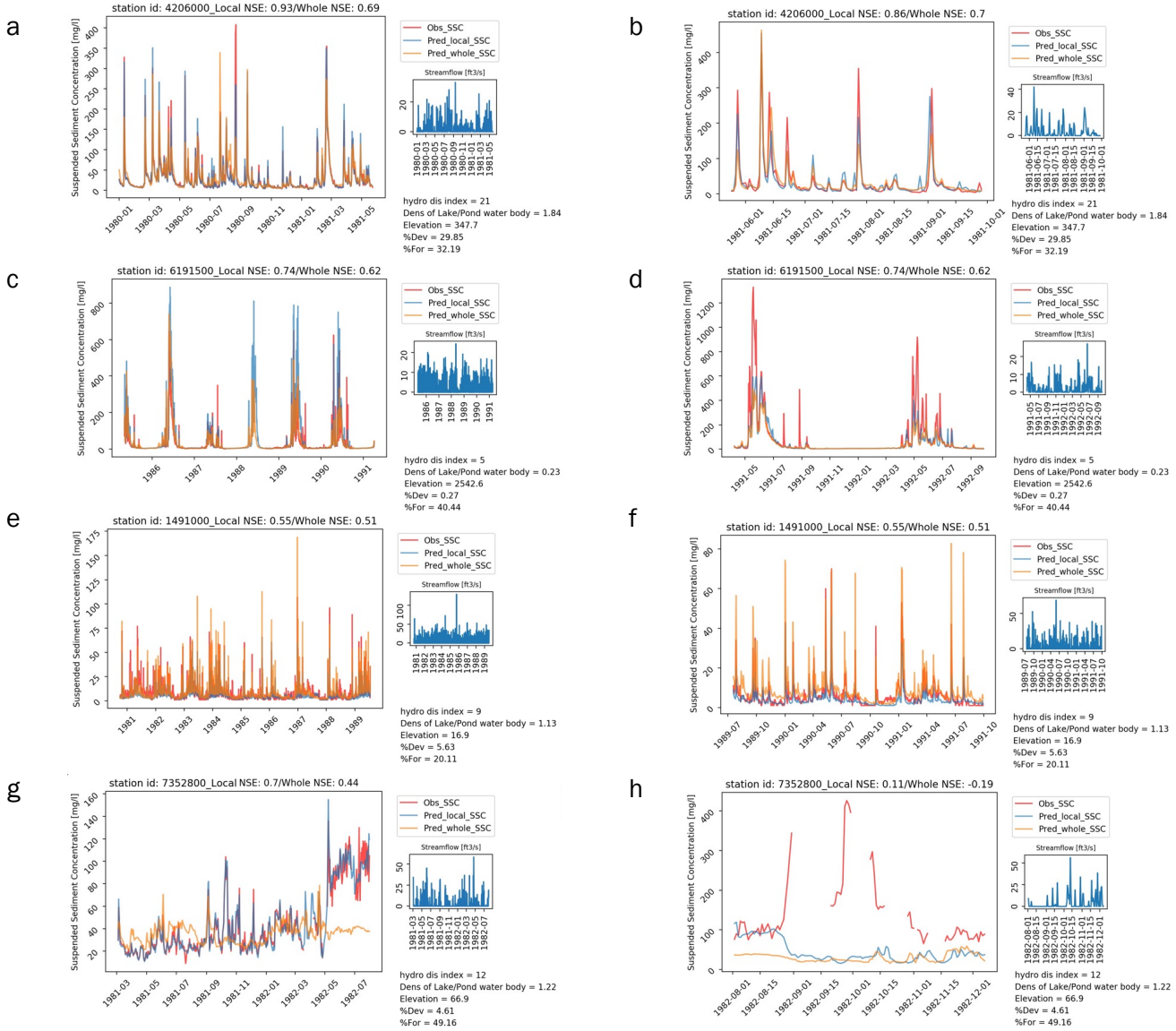

Figure 25 Time-Series plot for selected sites from the Whole-CONUS (all sites): a,c,e, and g are the plot from training sessions of sites chosen from the Very Good tier, Good tier, Satisfied tier, and Unsatisfied tier, respectively. b,d,f, and h are the plot from testing sessions of selected sites from the Very Good tier, Good tier, Satisfied tier, and Unsatisfied tier, respectively

The 2nd research question: Can the trained model learn to predict ungauged areas?

To answer this question, the Whole-CONUS ungauged predictions experiment was developed. For the Whole-CONUS approach with the 284-basin training set, there are 63 stations with an NSE < 0.4 (22 percent of the 377 stations available), 131 stations with 0.4 < an NSE < 0.7 (46 percent), and there are 90 stations with NSE > 0.8 (32 percent). Time-series plots for selected sites and the Whisker-box plot of the experiment are shown below.

The results from the Whole-CONUS approach with the 93-ungauged-basin testing can be ranked in the same tier as the 377-basin and the 284-basin model as it shows a median NSE of 0.521. The result clearly indicates that the trained Whole-CONUS model holds the capability to predict ungauged sites with satisfying performance.

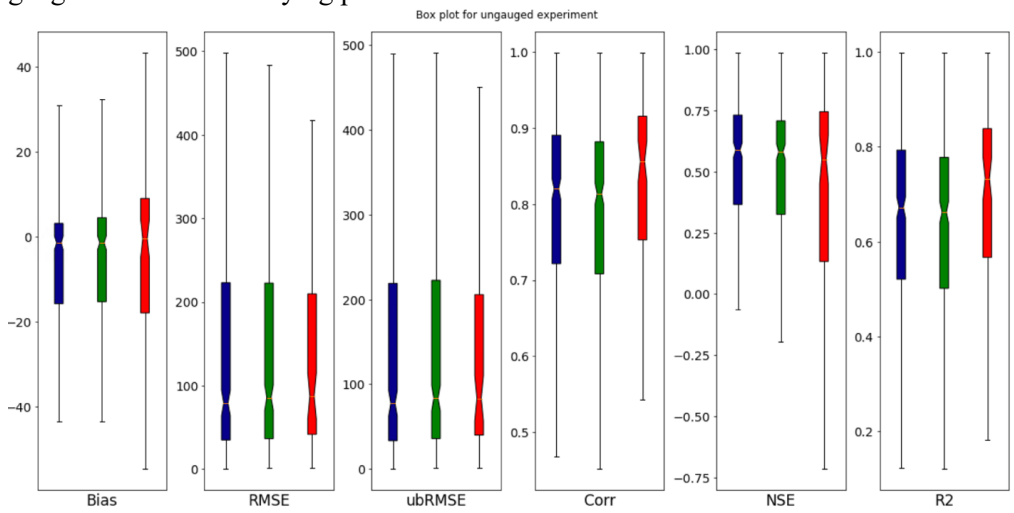

Figure 26 The Box plot of the Whole-CONUS (ungauged experiment): Blue is the Whole-CONUS model with 284 in a training session performance; Green is the Whole-CONUS model with 284 in a testing session performance; Red is the Whole-CONUS model with 93-ungauged-sites testing performance

Table 8 Number of sites' performance distributed in each criterion

Model/session	NSE < 0.45 (Unsatisfactory)	0.45< NSE ≦ 0.7 (Satisfactory)	0.7 < NSE ≦ 0.8 (Good)	NSE > 0.8 (Very good)
Whole-CONUS with 284 sites training /Training	80	118	48	38
Whole-CONUS with 284 training /Testing	91	119	45	29
Ungauged sites (93 sites)/ Testing	30	35	12	16

Chapter 5

Limitations and future works

Limitations

In this study, 380 models were developed (377 Local-CONUS models and 3 Whole-CONUS models). The LSTM-based sediment model holds a strong capability in suspended sediment concentration prediction, especially in the rich-data basin. Further, as the Whole-CONUS model reflects a satisfactory performance on large-scale prediction in both experiments (All-sites and Ungauged), the Whole-CONUS model can be considered as a suspended sediment concentration prediction tool in ungauged areas, which only needs hydrometeorological forcing, static watershed attributes, and streamflow discharge to predict suspended sediment concentration. Nevertheless, since both Local-CONUS and Whole-CONUS were trained with the specific products from DAYMET, GAGES-II, and streamflow, there are a few limitations of these models, which are discussed in the following paragraph.

Data availability of inputs limits the number of sites that can be trained and predict suspended sediment concentration.

Data availability has been an issue for Deep Learning communities for a long time, and the trend has continued in this study as well. Although such inputs as hydrometeorological forcing and streamflow are not an issue for our case because they are satellite-based products, and streamflow can be simulated using the LSTM-based model (Ouyang et al., 2021), suspended sediment concentration observations and static watershed attributes are controlled as described by the following two limitations.

The first point is that the models require daily suspended sediment concentration observations and static watershed attributes to be available for the training process. Although there are 9,312 available sites from the GAGES-II datasets, its paucity of suspended sediment concentration limits the number of basins across the CONUS that can be used (in this case, only 377 sites). The availability of SSC and the static attributes need to be available at the same site at the same time.

The second point is that, in the same way, the models have been trained with the static watershed attributes from the GAGES-II product, which holds 9,312 basins. Thus, in prediction, both gauged and ungauged sites across the Contiguous United States are limited to these 9,312 sites.

Data availability limits the training performance of the model.

Even though there are no "golden" rules for testing dataset size, at least 45 data points (for training 30 days and testing 15 days, as an approximate 70:30 training to testing ratio) are required for each site. Because the 45-day SSC requirement will limit the hyperparameter rho, and this hyperparameter will define sampling processes from the data pool in training (rho cannot exceed the available range of data described in no_days in Table 3 in Appendix). A lower magnitude of rho will lead to a higher computational time (a higher number of iterations in one epoch). For the current setting, the Local-CONUS models use about three days and fifteen hours to train and test for all 377 sites, and the Whole-CONUS model used approximately four days to train and test.

Future works

As a hunger modeler, the median of NSE from the Whole-CONUS (0.596) is still far behind the median of NSE from Local-CONUS (0.687), suggesting the current configuration partially reflects the issue of uncaptured spatial heterogeneity; one Whole-CONUS model alone can't reach the same exceptional performance as the individual Local-CONUS models.

The author hypothesizes that the lower performance from the Whole-CONUS model are due to a few factors:

1. Lacking information on spatial watershed characteristics from the static watershed attributes to overcome the non-stationary, non-linear, hysteresis.
2. Lacking tuning to reflect the optimized version of the Whole-CONUS model to solve the suspended sediment concentration problem (higher hidden size? Higher batch size?)

Gaining more information on spatial characteristics from the static watershed attributes to overcome the non-stationary, non-linear hysteresis.

Gaining more spatial heterogeneity knowledge from site to site across the CONUS may require more static watershed attributes, which are related to the geospatial characteristic of basins. A current list of static watershed attributes can be found in Table 2 in Appendix. The selected attributes are chosen from 5 categories: (1). Geospatial and topographic parameters (Elevation, Drainage area, Slope, etc.); (2) River fragmentation (Dam storage, Fragmentation index, etc.); (3) River characteristics (Stream density); (4) land use and land covers (Percent of the forest, Percent

of development, Percent of different types of soil, Hydraulic conductivity, etc.); (5) Hydrological parameters (The mean of precipitation, Rainfall and Runoff ratio, etc.).

Future work should focus on the 1st category (Geospatial and topographic parameters) such as the mean aspect, aspect of the northness, and aspect of the eastness for each basin's Hydrologic Landscape Region (HLRs are aggregates of watersheds that have been grouped according to their similarities in land-surface form, geologic texture, and climate characteristics (Winter (2001)).

Hyperparameter tuning to the optimized version of the Whole-CONUS to solve the suspended sediment concentration problem

Although, from the author's intuition, hyperparameter tuning will likely not significantly improve the model's performance, the author believes the model performance can still be improved. The Hidden size of the model should be increased to make the model more complex, and the batch size should be raised to let the model learn a higher number of sites in one epoch, leading to a higher learning rate.

References

A. K Lohani , N. K. G. K. K. S. B. (2007). Deriving stage–discharge–sediment concentration relationships using fuzzy logic.

Aboalhasan Fathabadi, S. M. S., Arash Malekian. (2022). Comparison of Bayesian, k-Nearest Neighbor and Gaussian process regression methods for quantifying uncertainty of suspended sediment concentration prediction.

Ajai Singh, M. I., R. K. Isaac, and D. M. Denis. (2013). Comparison of Artificial Neural Network Models for Sediment Yield Prediction at Single Gauging Station of Watershed in Eastern India.

Alp, H. K. C. a. M. (2006). Generalized regression neural network in modelling river sediment yield.

Andalib, V. N. a. G. (2015). Daily and Monthly Suspended Sediment Load Predictions Using Wavelet Based Artificial Intelligence Approaches.

Anurag Malik, A. K., Ozgur Kisi, and Jalal Shiri. (2019). Evaluating the performance of four different heuristic approaches with Gamma test for daily suspended sediment concentration modeling.

Arvind Yadav, S. C., and Sk. Md. Equeenuddin. (2018). Suspended sediment yield estimation using genetic algorithm-based artificial intelligence models: case study of Mahanadi River, India.

Ashish Kumar, P. K., Vijay Kumar Singh. (2019). Evaluating Different Machine Learning Models for Runoff and Suspended Sediment Simulation.

Avinash Agarwal, R. S., SK Mishra, and PK Bhunya. (2005). ANN-based sediment yield models for Vamsadhara
river basin (India).

B. B. Hazarika, D. G., M. Berlin. (2020). A coiflet LDMR and coiflet OB-ELM for river suspended sediment load prediction.

Banadkooki, F. B., Ehteram, M., Ahmed, A. N., Teo, F. Y., Ebrahimi, M., Fai, C. M., . . . El-Shafie, A. (2020a). Correction to: Suspended sediment load prediction using artificial neural network and ant lion optimization algorithm. *Environ Sci Pollut Res Int, 27*(30), 38117-38119. doi:10.1007/s11356-020-10139-x

Banadkooki, F. B., Ehteram, M., Ahmed, A. N., Teo, F. Y., Ebrahimi, M., Fai, C. M., . . . El-Shafie, A. (2020b). Suspended sediment load prediction using artificial neural network and ant lion optimization algorithm. *Environ Sci Pollut Res Int, 27*(30), 38094-38116. doi:10.1007/s11356-020-09876-w

Barenya Bikash Hazarika, D. G., Mohanadhas Berlin. (2020). Modeling suspended sediment load in a river using extreme learning machine and twin support vector regression with wavelet conjunction.

Bestami Taşar, Y. Z. K., Hakan Varçin, Fatih Üneş, Mustafa Demirci. (2017). Forecasting of Suspended Sediment in Rivers Using Artificial Neural Networks Approach.

Beven, K. (2006). A manifesto for the equifinality thesis.

Bonakdari, H. M. a. (2017). Impact of Normalization and Input on ARMAX-ANN Model Performance in Suspended Sediment Load Prediction.

Chetlur, S., Woolley, C., Vandermersch, P., Cohen, J., Tran, J., Catanzaro, B., & Shelhamer, E. (2014). cudnn: Efficient primitives for deep learning. *arXiv preprint arXiv:1410.0759*.

Choubin, B., Darabi, H., Rahmati, O., Sajedi-Hosseini, F., & Kløve, B. (2018). River suspended sediment modelling using the CART model: A comparative study of machine learning techniques. *Science of The Total Environment, 615*, 272-281. doi:https://doi.org/10.1016/j.scitotenv.2017.09.293

Cigizoglu, H. K. (2004). Estimation and forecasting of daily suspended sediment data by multi-layer perceptrons. *Advances in Water Resources, 27*(2), 185-195. doi:https://doi.org/10.1016/j.advwatres.2003.10.003

Cronin, D. S. v. M. a. K. (2016). Uncertainty in complex three-dimensional sediment transport models: equifinality in a model application of the Ems Estuary, the Netherlands.

Dapeng Feng, K. F., and Chaopeng Shen. (2020). Enhancing streamflow forecast and extracting insights using continental-scale long-short term memory networks with data integration.

Dheeraj Kumar, A. P., Nayan Sharma, Wolfgang-Albert Flügel. (2016). Daily suspended sediment simulation using machine learning approach.

Ehsan Olyaie, H. B., Kwok-Wing Chau, and Assefa M. Melesse. (2014). A comparison of various artificial intelligence approaches performance for estimating suspended sediment load of river systems: a case study in United States.

Elnaz Sharghi, V. N., Hessam Najafi and Huseyin Gokcekus. (2019). Conjunction of a newly proposed emotional ANN (EANN) and wavelet transform for suspended sediment load modeling.

Fatih Üneş, B. T., Mustafa Demirci, Martina Zelekova, Yunus Ziya Kaya, Hakan Varçin. (2021). Daily Suspended Sediment Prediction Using Seasonal Time Series and Artificial Intelligence Techniques.

G. Grill, B. L., M. Thieme, B. Geenen, D. Tickner, F. Antonelli, S. Babu, P. Borrelli, L. Cheng, H. Crochetiere,, H. Ehalt Macedo, R. F., M. Goichot, J. Higgins, Z. Hogan, B. Lip, M. E. McClain16,17, J. Meng, M. Mulligan,, C. Nilsson, J. D. O., J. J. Opperman, P. Petry, C. Reidy Liermann, L. Sáenz, S. Salinas-Rodríguez, P. Schelle,, & R. J. P. Schmitt, J. S., F. Tan, K. Tockner, P. H. Valdujo, A. van Soesbergen, and C. Zarfl. (2019). Mapping the world's free-flowing rivers.

Gal, Y., & Ghahramani, Z. (2016). *Advances in Neural Information Processing Systems* (Vol. 29).

Ganasri, B. P., & Gowda, R. (2015). Assessment of soil erosion by RUSLE model using remote sensing and GIS - A case study of Nethravathi Basin. *Geoscience Frontiers, 7*. doi:10.1016/j.gsf.2015.10.007

Goyal, M. K. (2014). Modeling of Sediment Yield Prediction Using M5 Model Tree Algorithm and Wavelet Regression.

Gu¨ngo¨r, M. F. a. M. (2010). Monthly total sediment forecasting using adaptive neuro fuzzy inference system.

Hai Tao, B. K., Zaher Mundher Yaseen. (2019). The Feasibility of Integrative Radial Basis M5Tree Predictive Model for River Suspended Sediment Load Simulation.

Hamid Darabi, S. M., Zahra Karimidastenaei, Ozgur Kisi, Mohammad Ehteram, Ahmed ELShafie, and Ali Torabi Haghighi. (2021). Prediction of daily suspended sediment load (SSL) using new optimization algorithms and soft computing models.

Hong-Yi Li, Z. T., Hongbo Ma, Zhenduo Zhu, Guta Wakbulcho Abeshu, Senlin Zhu, Sagy Cohen,Tian Zhou, Donghui Xu, and L. Ruby Leung. (2022). A new large-scale suspended sediment model and its application over the United States.

Isa, M. R. M. R. B. R. S. S. M. H. (2012). River Suspended Sediment Prediction Using Various Multilayer Perceptron Neural Network Training
Algorithms—A Case Study in Malaysia.

Isa, M. R. U. M. a. M. H. (2014). Comparative Study of MLP and RBF Neural Networks for Estimation of Suspended Sediments in Pari River, Perak.

Kai Ma, D. F., Kathryn Lawson, Wen-Ping Tsai, Chuan Liang, Xiaorong Huang, Ashutosh Sharma, and Chaopeng Shen. (2021). Transferring hydrologic data across continents leveraging data-rich regions to improve hydrologic prediction in data-sparse regions.

Keivan Kaveh, M. D. B., Peter Rutschmann. (2017). A comparative study of three different learning algorithms applied to ANFIS for predicting daily suspended sediment concentration. .

Kenneth Renard, G. F., Glenn Weesies, and Jeffrey Porter. (1991). Revised universal soil loss equation.

Kisi, O. (2005). Suspended sediment estimation using neurofuzzy and neural network approaches.

Kisi, O. (2008). Constructing neural network sediment estimation models using a data-driven algorithm.

Kuai Fang, D. K., Dapeng Feng, Kathryn Lawson and Chaopeng Shen. (2022). The data synergy effects of time-series deep learning models in hydrology.

Kuai Fang, D. K., Kathryn Lawson, and Chaopeng Shen. (2020). Evaluating the Potential and Challenges of an Uncertainty Quantification Method for Long Short-Term Memory Models for Soil Moisture Predictions.

Lei Wu, X. L., Junlai Chen, Yang Yu, Xiaoyi Ma. (2022). Overcoming equifinality: time-varying analysis of sensitivity and identifiability of SWAT runoff and sediment parameters in an arid and semiarid watershed.

Leopold, G. (2017). Nvidia's Huang Sees AI 'Cambrian Explosion'. Retrieved from https://www.datanami.com/2017/05/24/nvidias-huangsees-ai-cambrian-explosion/

Leopold, L. B., & Wolman, M. G. (1957). *River channel patterns: Braided, meandering, and straight* (282B). Retrieved from Washington, D.C.: http://pubs.er.usgs.gov/publication/pp282B

Leopold, L. B., Wolman, M. G., & Miller, J. P. (1964). *Fluvial processes in geomorphology*. New York, NY: Dover Publications, Inc.

Liu, P., Wang, J., Sangaiah, A. K., Xie, Y., & Yin, X. (2019). Analysis and Prediction of Water Quality Using LSTM Deep Neural Networks in IoT Environment. *Sustainability, 11*(7), 2058.

Melesse, A. M., Ahmad, S., McClain, M. E., Wang, X., & Lim, Y. H. (2011). Suspended sediment load prediction of river systems: An artificial neural network approach. *Agricultural Water Management, 98*(5), 855-866. doi:https://doi.org/10.1016/j.agwat.2010.12.012

Milliman, J. P. M. S. a. J. D. (2007). Geology, Geography, and Humans Battle for Dominance over the Delivery of Fluvial Sediment to the Coastal Ocean.

Mohammad Zounemat-Kermani, Ö. r. K., Jan Adamowski, Abdollah Ramezani-Charmahineh. (2016). Evaluation of data driven models for river suspended sediment concentration modeling.

Morgan, R. P. C. (2001). A simple approach to soil loss prediction: a revised Morgan–Morgan–Finney model.

Murat Alp, H. K. C. (2007). Suspended sediment load simulation by two artificial neural network methods using hydrometeorological data.

Nouar AlDahoul, Y. E., Pavitra Kumar, Ali Najah Ahmed, Mohsen Sherif,, & Ahmed Sefelnasr, a. A. E. (2021). Suspended sediment load prediction using long short-term memory neural network.

Opperman , J. J., Moyle , P. B., Larsen , E. W., Florsheim, J. L., & Manfree, A. D. (2017). *Floodplains Processes and Management for Ecosystem Services*. USA: University of California Press.

Paszke, A., Gross, S., Massa, F., Lerer, A., Bradbury, J., Chanan, G., . . . Antiga, L. (2019). *Advances in Neural Information Processing Systems*.

Pellerin, B. A., Stauffer, B. A., Young, D. A., Sullivan, D. J., Bricker, S. B., Walbridge, M. R., . . . Shaw, D. M. (2016). Emerging tools for continuous nutrient monitoring networks: Sensors advancing science and water resources protection. *J. Am. Water Resour. Assoc., 52*(4), 993.

Pena, M., Katsev, S., Oguz, T., & Gilbert, D. (2010). Modeling dissolved oxygen dynamics and hypoxia. *Biogeosciences, 7*(3), 933.

Poole, G. C., & Berman, C. H. (2001). An Ecological Perspective on In-Stream Temperature: Natural Heat Dynamics and Mechanisms of Human-CausedThermal Degradation. *Environ. Manage., 27*(6), 787.

Puri, R., Khadka, K., & Paudyal, A. (2013). Separating climate resilient crops through screening of drought tolerant rice land races in Nepal. *Agronomy Journal of Nepal, 1*. doi:10.3126/ajn.v1i0.7546

Q.J. Liu, H. Y. Z., K.T. Gaoc, B. Xu, J.Z. Wu, N.F. Fang. (2019). Time-frequency analysis and simulation of the watershed suspended sediment concentration based on the Hilbert-Huang transform (HHT) and artificial neural network (ANN) methods: A case study in the Loess Plateau of China.

Rabalais, N. N., Turner, R. E., & Wiseman, W. J. (2002). The Dead Zone. *Annu. Rev. Ecol. Syst., 33*(1), 235.

Rahmani, F., Lawson, K., Ouyang, W., Appling, A., Oliver, S., & Shen, C. (2020). Exploring the exceptional performance of a deep learning stream temperature model and the value of streamflow data. *Environ. Res. Lett.*

Rowan, K. B. a. J. (2000). Equifinality and uncertainty in physically based soil erosion models: application of the GLUE methodology to WEPP-the Water Erosion Prediction Project-for sites in the UK and USA.

Sadra Shadkani, A. A., Saeed Samadianfard, Sajjad Hashemi, Amirhosein Mosavi, Shahab S. Band. (2020). Comparative study of multilayer perceptron-stochastic gradient descent and gradient boosted trees for predicting daily suspended sediment load: the case study of the Mississippi RiverU.S.

Sagy Cohen, A. J. K., James P.M. Syvitski. (2014). Global suspended sediment and water discharge dynamics between 1960 and 2010: Continental trends and intra-basin sensitivity.

Sagy Cohen, A. K., JamesP.M.Syvitski, Bala´ zs M.Fekete. (2013). WBMsed, a distributed global-scale riverine sediment flux model: Model description and validation.

Sarita Gajbhiye Meshram, M. A. G., Ravinesh C. Deo, Mahsa Hasanpour, & Kashani, C. M., Vahid Karimi. (2019). New Approach for Sediment Yield Forecasting with a Two-Phase Feedforward Neuron Network-Particle Swarm Optimization Model Integrated with the Gravitational Search Algorithm.

Shen, K. F. a. C. (2020). Near-real-time forecast of satellite-based soil moisture using long short-term memory with an adaptive data integration kernel.

T. Francke, J. A. L. o.-T. o., and B. Schr¨oder1. (2008). Estimation of suspended sediment concentration and yield using linear models, random forests and quantile regression forests.

Taher Rajaee, S. A. M., Mohammad Zounemat-Kermani, and Vahid Nourani. (2009). Daily suspended sediment concentration simulation using ANN and neuro-fuzzy models.

Thomas, C. W. (2001). The concept of Hydrologic Landscapes.

V. Jothiprakash and Vaibhav Garg. (2009). Reservoir Sedimentation Estimation Using Artificial Neural Network.

Vahid Nourani, A. M., Ali Davanlou Tajbakhsh, Hessam Najafi. (2019). A Wavelet Based Data Mining Technique for Suspended Sediment Load Modeling.

Wen-ping Tsai, D. F., Ming Pan, Hylke Beck, Kathryn Lawson, Yuan Yang, Jiangtao Liu, and Chaopeng Shen. (2021). From calibration to parameter learning: Harnessing the scaling effects of big data in geoscientific modeling.

Wen-ping Tsai, K. F., Xinji Ye, Kathryn Lawson and Chaopeng Shen. (2020). Revealing causal controls of storage-streamflow relationships with a data-centric Bayesian framework combining machine learning and process-based modeling.

Wohl, E. (2020). Rivers in landscape.

Wohl, E., Bledsoe, B. P., Jacobson, R. B., Poff, N. L., Rathburn, S. L., Walters, D. M., & Wilcox, A. C. (2015). The Natural Sediment Regime in Rivers: Broadening the Foundation for Ecosystem Management. *Bioscience, 65*(4), 358-371. doi:10.1093/biosci/biv002

Xiang Li, A. K., Xiaowei Jia, Kelly Cutler, Rahul Ghosh, Arvind Renganathan, Shaoming Xu, J L Nieber, Christopher J Duffy, Michael Steinbach, and Vipin Kumar. (2022). Regionalization in a global hydrologic deep learning model: from physical descriptors to random vectors.

Appendix A

Sediment models studies in the last decades

Table 9 Sediment models studies in the last decades

Publications	Models/compared with	Inputs	Target	Study area	Training/ Testing	Time scale	Training Performance	Testing Performance	Remark
Cigizoglu (2004)	MLP/SRC	SSL, Discharge	SL [tons/day]	Schuylkill river (USGS code: 1470500 and 1473800)	1952 - 1978/ 1979 - 1981	Daily	-	MSE = 34 x 10^6 tons2/day2 R2 = 0.27	-
Agarwal et al., 2005	FFNN (LTF, BPANN)	SSC, rainfall, discharge	SSC [mg/L]	Vamsadhara River basin up to Kashinagar, India	1984 - 1989/ 1992 - 1995	Daily, Weekly, Ten-daily, and monthly	Daily RMSE = 199, R2 = 0.871 , E = 0.712 Weekly RMSE = 766 R2 = 0.908 E = 0.777 Ten-daily RMSE = 833 R2 = 0.935 E = 0.830 Monthly RMSE = 1,404 R2 = 0.940 E = 0.859	• ** Daily RMSE = 308 R2 = 0.850 E = 0.574 • ** Weekly RMSE = 1433 R2 = 0.874 E = 0.636 • ** Ten-daily RMSE = 1828 R2 = 0.871 E = 0.638 • ** Monthly RMSE = 3,988 R2 = 0.834 E = 0.513	Linear Transfer Function, Back Propagation Artificial Neural Network **There are two testing periods, only the best period with the best performances are shown

Kisi 2005	Neuro-Fuzzy/SRC	SSC, Discharge	SSC [mg/L]	Quebrada Blanca (USGS: 50051150) and Rio Valenciano (USGS: 50056400)	1994/ 1995	Daily	-	**MRSE =2.72 **R2 = 0.876	**The best performance from one inputs combination
Cigizoglu and Alp (2006)	FFBP, GRNN/MLR, SRC	SSL, Discharge	SSL [mg/day]	Juniata River, Pennsylvania [USGS code: 01567000]	1983 - 1988/ 1988 - 1989	Daily	-	**MSE = 29,211 **R2 = 0.958	Feed Forward Back Propagation algorithm **The best performance from one set of inputs combination
Alp and Cigizoglu (2007)	FFBP/RBF	SSL, rainfall, discharge	SSL [tons/day]	Juniata River, Pennsylvania [USGS code: 01567000]	1983 - 1988/ 1988 - 1989	Daily	-	• **For FFBP MSE = 124,997 R2 = 0.864 • **For RBF MSE = 118,496 R2 = 0.868	Radial Function-based Neural Network **The best performance from one set of inputs combination
Lohani et al., 2007	ANN, FL/ SRC	SSC, Discharge	SSC [mg/L]	Jamtara river, India	250 days/ 156 days	Daily	-	**R = 0.815 **RMSE = 82.83	**The best performance from one inputs combination
Francke et al., 2008	Generalized Linear Models, RF, Quantile RF	SSC, Discharge	SSC [g/L]	subcatchments in Isebana (Torrelaribera, Villacarli, Cabecera, and Capella), Central Spanish Pyrenees	Sep - Dec 2006 (Does not mention training and testing period)	Daily	-	•**Torrelaribera RMSE = 29.98 R = 0.74 • **Villacarli RMSE = 25.85 R = 0.64 • **Cabecera RMSE = 5.73 R = 0.39 • **Capella RMSE = 17.15 R = 0.13	**The best performance from one set of inputs combination

Kisi 2008	ANN with Levenberg–Marquardt (LM), Conjugate gradient (CG) /SRC	SSC, Discharge	SSC [mg/L]	Quebrada Blanca (USGS: 50051150) and Rio Valenciano (USGS: 50056400)	1994/ 1995	Daily	• For LM MRSE = 75 R2 = not reported • For CG MRSE = 156 R2 = not reported	• For LM MRSE = 83 R2 = 0.964 • For CG MRSE = 167 R2 = 0.937	**The best performance among configurations
Jothiprakash and Garg (2009)	MLP/-	Rainfall, inflow, reservoir capacity, sediment volume	Volume of sediment retained	Satluj River, India	Randomly selected 70% of available data. The remaining 30% for testing.	Yearly	R = 0.970 RMSE = 2.612 x 10^6 m3 MAE = 2.264 x10^6 m3 AARE = 0.305 E = 0.927	R = 0.965 RMSE = 3.513 x 10^6 m3 MAE = 3.143 x10^6 m3 AARE = 1.181 E = 0.890	-
Rajaee et al., 2009	ANN, NF, MLR/ SRC	SSC, Discharge	SSC [mg/L]	Little black river (USGS code: 07068510), Salt river (USGS code: 05508000)	• Little Black river: Oct 1980 - Sep 1983/ Oct 1983 - Sep 1984 • Salt river: Oct 1984 - Sep 1987/ Oct 1987 - Sep 1988	Daily	• **Little Black river RMSE = R = 0.390 • **Salt river RMSE = R =	• ** ANN Little Black river RMSE = 21.41 R2 = 0.457 Salt river RMSE = 66.15 R2 = 0.345 • **NF Little Black river RMSE = 15.98 R2 = 0.697 Salt river RMSE = 61.41 R2 = 0.435 • **MLR Little Black river RMSE = 25.04 R2 = 0.257 Salt river RMSE = 69.16 R = 0.284 • **SRC Little Black river RMSE = 25.6 R2 = 0.225 Salt river RMSE = 75.7 R2 = 0.144	**The best performance from one set of inputs combination

Firat and Gungor 2010	ANFIS/ANN, MLR			Aydın Bridge (706), Menderes C¸ ıtak Ko¨pru (713), and Do¨rt Deg¨irmen (735) in Great Menderes, Anatolia	Testing with 3 years and the remain of available data is a training	Monthly	-	• **706 NRMSE = 0.649 NSE = 0.742 R = 0.866 • **713 NRMSE = 0.747 NSE = 0.787 R = 0.893 • **735 NRMSE = 0.824 NSE = 0.769 R = 0.914	**The best performance from one set of inputs combination
Melesse et al., 2011	FFNN (Feed Forward Neural Network)/MLR, ARIMA (Autoregressive Integrated Moving Average), MNLP	SSL, rainfall, discharge	SSL [mg/day]	Mississippi, Missouri and Rio Grande rivers	1971 -1973 / 1974 - 1975 [Mississipi], 1977 - 1979/ 1980 - 1981 [Missouri and Rio Grande]	Daily and Weekly	-	• **For ANN (Daily), [Mississipi] RMSE= 54,928 MAPE = 11.7 E =0.80 R2 = 0.96 • **For ANN (Weekly), [Mississipi] RMSE= 677,031 MAPE = 16.8 E = 0.60 R2 = 0.87	**The best performance among configurations

							-	• **For ANN (Daily), [Missouri] RMSE = 54,928, MAPE = 11.7, E = 0.80, R2 = 0.96 • **For ANN (Weekly), [Missouri] RMSE= 54,928, MAPE = 11.7, E =0.80, R2 = 0.96	-
							-	• **For ANN (Daily), [Rio Grande] RMSE = 2,072 MAPE = 114.5, E = 0.46 R2 = 0.65 • **For ANN (Weekly), [Rio Grande] RMSE= 17,907 MAPE = 112.5 E = 0.25 R2 = 0.40	-

Mustafa et al., 2012	MLP/-	SSL, Discharge	SSL [tons/day]	Pari river, Malaysia	1993 - 1998 [70:30]	Daily	• Gradient Descent R2 = 0.9846 , RMSE = 253, MARE = 0.227 • Gradient Descent Momentum R2 = RMSE = 254, MARE = 0.228	• Gradient Descent R2 = 0.9837 RMSE = 106 MARE = 0.227 • Gradient Descent Momentum R2 = RMSE = 105, MARE = 0.228	-
Singh et al., 2013	SBP/RBNN	Rainfall, Runoff, and Sediment yield	Sediment yield [ton/ha]	Sewani river, India	1991 - 2004/ 2005 - 2007	Daily	-	**R2 = 0.81 **E = 0.90 **RMSE = 3,145.1	**The best performance from one set of inputs combination
Afan et al., 2014	FFNN/RBF	SSL, discharge	SSL [tons/day]	Johor River, Malaysia	3653 days/ 365 days	Daily	-	• **FFNN RMSE = 27.157 MAE = 19.144 R2 = 0.9031 • **RBF RMSE = 26.811 MAE = 17.343 R2 = 0.8991	RBF: Radial Basis Function **The best performance from one set of inputs combination
Goyal (2014)	M5T, BPANN	Rainfall, Discharge	Monthly sediment yield	Nagwa, India	1993 - 2004/ 2004 - 2007	Daily	-	• **M5T RMSE = 0.92 NSE = 0.79 R = 2920.46 • **BPANN RMSE = 2140 NSE = 0.68 R = 0.89	-
Mustafa and Isa (2014)	MLP/ RBF	SSL, Discharge	SSL [tons/day]	Pari river, Malaysia	1993 - 1998 [70:30]	Daily	• MLP RMSE = 47 MAE = 29 R2 = 0.9971 • RBF RMSE = 265 MAE = 57 R2 = 0.9091	• MLP RMSE = 62 MAE = 40 R2 = 0.9895 • RBF RMSE = 61 MAE = 41 R2 = 0.9898	

Olyaie et al., 2014	ANFIS/ANN, SRC	SSL, Discharge	SSL [tons/day]	Flathead British, MO (USGS code: 12355000) and Santa Clara (USGS code: 111080500)	• Flathead 75% / 25% of available data (1975-1981) • Santa Clara 75% / 25% of available data (1968-1974)	Daily	-	• ANFIS RMSE = [421.71, 218.37] MAPE = [0.3265, 0.2634] R = [0.867, 0.888] NSE = [0.750, 0.732] • ANN RMSE = [480.1, 240.9] MAPE = [0.5090, 0.3691] R = [0.813, 0.877] NSE = [0.694, 0.749] • SRC RMSE = [529.3, 280.7] MAPE = [0.6987, 0.6327] R = [0.673, 0.737] NSE = [0.602, 0.505]	**The best performance from one set of inputs combination
Nourani and Andalib 2015	LSSVM, WANN	SSL, Discharge	SSL	Thebes, Mississippi river	75% / 25% of available data	Daily and Monthly	•**LSSVM (Daily) RMSE = 0.019 R2 = 0.92 • **WANN (Daily) RMSE = 0.15 R2 = 0.92 • **LSSVM (Monthly) RMSE = 0.080 R2 = 0.71 • **WANN (Monthly) RMSE = 0.077 R2 = 0.74	• **LSSVM (Daily) RMSE = 0.015 R2 = 0.92 • **WANN (Daily) RMSE = 0.019 R2 = 0.96 • **LSSVM (Monthly) RMSE = 0.071 R2 = 0.70 • **WANN (Monthly) RMSE = 0.069 R2 = 0.72	-

Kumar et al., 2016	ANN-LM, RBFNN, CART, M5/ LSSVR	SSC, rainfall, discharge	SSC [mg/L]	Kopili river and Brahmaputra, India	70% / 30% of available data	Daily	• ANN R = 0.996 NSE = 0.9921 RSR = 0.291 • RBFNN R = 0.997 NSE = 0.99315 RSR = 0.053 • CART R = 0.99 NSE = 0.9913 RSR = 0.06 • LSSVR R = 0.923 NSE = 0.9887 RSR = 0.070 • M5 R = 0.92 NSE = 0.9918 RSR = 0.06	• ANN R = 0.921 NSE = 0.887 RSR = 0.291 • RBFNN R = 0.914 NSE = 0.847 RSR = 0.341 • CART R = 0.92 NSE = 0.8673 RSR = 0.32 • LSSVR R = 0.923 NSE = 0.8900 RSR = 0.072 • M5 R = 0.0.92 NSE = 0.8822 RSR = 0.29	**The best performance from one set of inputs combination

Zounemat-Kermani et al., 2016	ANN/ MLR, SRC	SSC, Discharge	SSC [mg/L]	Arkansas, Delaware, and Idaho	80% / 20% of available data	Daily	• Arkansus SRC RMSE = 281.513 SRC NSE = 0.1161 MLR RMSE = 261.309 MLR NSE = 0.2394 ANN RMSE = 255.399 ANN NSE = 0.2734 • Deleware SRC RMSE = 281.513 SRC NSE = 0.1161 MLR RMSE = 89.211 MLR NSE = 0.1635 ANN RMSE = 87.700 ANN NSE = 0.1986 • Idaho SRC RMSE = 20.746 SRC NSE = 0.8934 MLR RMSE = 261.309 MLR NSE = 0.2394 ANN RMSE = 14.924 ANN NSE = 0.9448	• Arkansus SRC RMSE = 237.810 SRC NSE = 0.1595 MLR RMSE = 213.353 MLR NSE = 0.3235 ANN RMSE = 206.531 ANN NSE = 0.3660 • Deleware SRC RMSE = 72.832 SRC NSE = 0.2746 MLR RMSE = 79.777 MLR NSE = 0.1297 ANN RMSE = 76.535 ANN NSE = 0.1980 • Idaho SRC RMSE = 37.166 SRC NSE = 0.1445 MLR RMSE = 21.589 MLR NSE = 0.7113 ANN RMSE = 15.417 ANN NSE = 0.8528	-
Kaveh et al., 2017	ANFIS	SSC, Discharge	SSC [mg/L]	Schuylkill river, PA (USGS code: 01473800)	Jan 1949 - Dec 1953 (83%) / Jan 1954 - Dec 1954 (17%)	Daily	-	• **ANFIS R2 = 0.7513 RMSE = 25.955 MAE = 11.859	**The best performance from one set of inputs combination

Tasar et al., 2017	MLR, M5T, ANN/ SRC	SSC, T, Discharge	SSC [mg/L]	Iowa station, USA (Does not report the USGS code)	70% / 30% of available data for each site	Daily	-	• **SRC MSE = 117877.4 MAE = 207.86 R = 0.5848 • **MLR MSE = 82268.13 MAE = 144.22 R = 0.8462 • **M5T MSE = 60883.11 MAE = 143.95 R = 0.8686 • **ANN MSE = 45242.93 MAE = 134.80 R = 0.8908	**The best performance from one set of inputs combination
Moeeni and Bonakdari 2017	ARMAX-ANN	SSL, Discharge	SSL [tons/day]	Pineville station and Barbourville station in Cumberland river, USA	October 1, 1979 - September 30, 1986/ October 1, 1986 - September 30, 1989	Daily	-	• ARMAX-ANN (Pineville) MAE = 604 R2 = 0.864 CRM = -0.210 VAF = 78.4 • ARMAX-ANN (Barbourville) MAE = 596 R2 = 0.885 CRM = -0.078 VAF = 80.3	-
Yadav et al., 2018	GA-ANN/ANN, SVM	SSL, Discharge, Rainfall, and Temperature	SSL [tons/month]	Mahanadi river, India	70%/ 30% of available data (1990 - 2005)	Monthly	• GA-ANN RMSE = 0.0554 R2 = 0.9267 MAE = 0.0267 • ANN RMSE = 0.0425 R2 = 0.9410 MAE = 0.0201 • SVM RMSE = 0.06118 R2 = 0.88456 MAE = 0.02432	• GA-ANN RMSE = 0.02675 R2 = 0.9923 MAE = 0.0146 • ANN RMSE = 0.0419 R2 = 0.9948 MAE = 0.0157 • SVM RMSE = 0.03442 R2 = 0.94755 MAE = 0.01896	-
Liu et al., 2019	ANN	Discharge, NDVI, Rainfall	SSC [mg/L]	Kuye river, China	2006 - 2008/ 2009 - 2010	Daily	-	**R2 = 0.64 **NSE = 0.63	**The best performance from one set of inputs combination

Kumar et al., 2019	ANN, ANFIS	Water stage, Discharge, SSC	SSC [mg/L]	Pathagudem, India	1996–2007/ 2008 - 2010	Daily	**R = 0.941 **RMSE = 0.1461 **R2 = 0.901 **PARE = -2xE-8	**R = 0.926 **RMSE = 0.1240 **R2 = 0.960 **PARE = -0.003	**The best performance from one set of inputs combination
Malik et al., 2019	RBNN, SOMNN, LSSVR/ SRC	SSC, Discharge	SSC [g/L]	Ashti station, Bahmini station , Tekra station, India	75% data from July 1, 2003 - August 31, 2010/ 25% data from September 1, 2010 - October 31, 2012	Daily	-	• **RBNN (Ashti) RMSE = 0.045 COE = 0.884 PCC = 0.955, WI = 0.970 • **RBNN (Bahmini) RMSE = 0.062 COE = 0.883 PCC = 0.961, WI = 0.963 • **RBNN (Tekra) RMSE = 0.131 COE = 0.914 PCC = 0.958 WI = 0.976	-
Meshram et al., 2019	ANFIS	Rainfall, Runoff	SSC [mg/L]	Narmady river, India	80% / 20% of available data ranging from 2000 - 2009	Monthly	MAE = 30,916.4 NSE = 0.524 WI index = 0.819	MAE = 19773.3 NSE = 0.419 WI index = 0.788	**The best performance from one set of inputs combination

Nourani et al., 2019	WANN, M5, and WANN-M5	SSL, Discharge	SSL [tons/day], SSL [tons/month]	Lightvachai river and Upper Rio Grande river	75% / 25% of available data for each site	Daily and Monthly	• **ANN (Daily) Lightvachai river NSE = 0.93 RMSE = 0.02 MAPE = 1.54 Upper Rio Grande NSE = 0.62 RMSE = 0.04 MAPE = 5.89 • **WANN (Daily) Lightvachai river NSE = 0.98 RMSE = 0.01 MAPE = 0.53 Upper Rio Grande NSE = 0.89 RMSE = 0.01 MAPE = 2.51 • **M5 (Daily) Lightvachai river NSE = 0.92 RMSE = 0.01 MAPE = 1.43 Upper Rio Grande NSE = 0.77 RMSE = 0.01 MAPE = 3.75 • **WANN-M5 (Daily) Lightvachai river NSE = 0.97 RMSE = 0.006 MAPE = 0.40 Upper Rio Grande NSE = 0.94 RMSE = 0.004 MAPE = 1.81 • **ANN (Monthly) Lightvachai river NSE = 0.61 RMSE = 0.07 MAPE = 1.23 Upper Rio Grande NSE = 0.44 RMSE = 0.09 MAPE = 3.15 • **WANN (Monthly) Lightvachai river NSE = 0.97 RMSE = 0.01 MAPE = 0.56 Upper Rio Grande NSE = 0.93 RMSE = 0.03 MAPE = 1.28 • **M5 (Monthly) Lightvachai river NSE = 0.78 RMSE = 0.02 MAPE = 0.83 Upper Rio Grande NSE = 0.68 RMSE = 0.04 MAPE = 0.06 • **WANN-M5 (Monthly) Lightvachai river NSE = 0.94 RMSE = 0.007 MAPE = 0.34 Upper Rio Grande NSE = 0.90 RMSE = 0.01 MAPE = 1.71	• **ANN (Daily) Lightvachai river NSE = 0.80 RMSE = 0.07 MAPE = 1.19 Upper Rio Grande NSE = 0.48 RMSE = 0.14 MAPE = 1.05 • **WANN (Daily) Lightvachai river NSE = 0.91 RMSE = 0.05 MAPE = 0.44 Upper Rio Grande NSE = 0.84 RMSE = 0.02 MAPE = 2.82 • **M5 (Daily) Lightvachai river NSE = 0.86 RMSE = 0.07 MAPE = 1.10 Upper Rio Grande NSE = 0.75 RMSE = 0.03 MAPE = 4.24 • **WANN-M5 (Daily) Lightvachai river NSE = 0.95 RMSE = 0.03 MAPE = 0.32 Upper Rio Grande NSE = 0.89 RMSE = 0.008 MAPE = 2.26 • **ANN (Monthly) Lightvachai river NSE = 0.48 RMSE = 0.14 MAPE = 1.05 Upper Rio Grande NSE = 0.30 RMSE = 0.14 MAPE = 4.61 • **WANN (Monthly) Lightvachai river NSE = 0.78 RMSE = 0.09 MAPE = 0.64 Upper Rio Grande NSE = 0.77 RMSE = 0.08 MAPE = 1.55 • **M5 (Monthly) Lightvachai river NSE = 0.69 RMSE = 0.07 MAPE = 0.70 Upper Rio Grande NSE = 0.70 RMSE = 0.06 MAPE = 3.15 • **WANN-M5 (Monthly) Lightvachai river NSE = 0.90 RMSE = 0.02 MAPE = 0.31 Upper Rio Grande NSE = 0.86 RMSE = 0.03 MAPE = 2.13	**The best performance from one set of inputs combination

Sharghi et al., 2019	WANN, EANN	SSL, Discharge	SSL [tons/days]	Lighvanchai, Azerbaijan and Upper Rio Grande Rivers, Colorado	75%/ 25% The time series data for 28 years, from 1987 to 2015 for the Lighvanchai River and 39 years, from 1976 to 2015 for Upper Rio Grande River	Daily, Monthly	•**WANNN Daily (Lighvanchai) RMSE = 2.123 NSE = 0.987 • **WANN Daily (Rio Grande) RMSE = 4516.79 NSE = 0.879 • **WANNN Monthly (Lighvanchai) RMSE = 305.156 NSE = 0.789 • **WANN Monthly (Rio Grande) RMSE = 12592.74 NSE = 0.742	**WANNN Daily (Lighvanchai) RMSE = 8.722 NSE = 0.915 • **WANN Daily (Rio Grande) RMSE = 7475.51 NSE = 0.781 • **WANNN Monthly (Lighvanchai) RMSE = 334.179 NSE = 0.779 • **WANN Monthly (Rio Grande) RMSE = 146935.55 NSE = 0.642	-
Tao et al., 2019	RM5Tree (M5 tree with Radial basis)/ MLR, RSM (Response Surface method), ANN, M5	SSL, Discharge	SSL [tons/day]	Delaware river, USA	8329 days/ 3569 days	Daily	-	• ** RM5Tree MAE = 427.2 RMSE = 2091.8 d = 0.929 NSE = 0.863	**The best performance from one set of inputs combination
Hazarlka et al., 2020	ELM, SVR	SSL, Discharge	SSC [g/L]	Tawang Chu River, Arunachal Pradesh	2013 - 2015 (not mentioned split training:testing ration)	Daily	-	• ** ELM RMSE = 0.042 MAE = 0.01063 • ** SVR RMSE = 0.0426 MAE = 0.15651	-

Shadkani et al., 2020	MLP, MLP-SGD, GBT	SSL, Discharge	SSL [tons/day]	St. Louis, MO (USGS code: 07010000) Chester, IL (USGS code: 07020500)	70% / 30% of available data (2004 - 2017)	Daily	-	• **MLP R2 = 0.982 NSE = 0.965 WI = 0.953 SI = 0.618 • **GBT R2 = 0.919 NSE = 0.957 WI = 0.949 SI = 0.618 • **MLP-SGD R2 = 0.932 NSE = 0.967 WI = 0.960 SI = 0.580	**The best performance from one set of inputs combination
Aldahoul et al., 2021	ElasticNetLR, XGB, MLP,and LSTM	SSL, Discharge	SSL [tons/day]	Johor River, Malaysia	80% / 20% of available data in 365 days	Daily, Weekly, Ten-daily, and monthly	-	• **LSTM Daily R2 = 0.9201 MAE = 12.55 RMSE = 22.92 RAE = 0.216 RSE = 0.079 • **LSTM Weekly R2 = 0.9656 MAE = 8.601 RMSE = 11.84 RAE = 0.187 RSE = 0.034 • **LSTM Ten-day R2 = 0.9671 MAE = 0.088 RMSE = 11.04 RAE = 0.183 RSE = 0.033 • **LSTM Monthly R2 = 0.9833 MAE = 2.447 RMSE = 3.236 RAE = 0.075 RSE = 0.005	**The best performance from one set of inputs combination

Darabi et al., 2021	MLP, ANFIS, RBF	SSC, Discharge	SSL [tons/day]	Talar river basin (Talar station) and Eagel Creek basin (Kasilian station)	80% / 20% of available data for each site	Daily	-	• ** Talar river basin RMSE = 934.2 NSE = 0.93 MAE = 912.2 PBIAS = 0.12 • ** Eagel Creek basin RMSE = 1412.10 NSE = 0.92 MAE = 1403.4 PBIAS = 0.14	**The best performance from one set of inputs combination
Hazarlka et al., 2021	coiflet LDMR, coiflet OB-ELM	SSL, Discharge	SSC [g/L]	Tawang Chu River, Arunachal Pradesh	70%/ 30% of available data (2013 - 2015)	Daily	-	• ** LDMR RMSE = 0.05339 MAE = 0.02414 • ** OB-ELM RMSE = 0.09091 MAE = 0.08503	Large margin distribution machine-based regression (LDMR)
Üneş et al., 2021	SRC, MLR, SVM-RBF, SVM-PK, LibSVM	SSC, Discharge	SSC [mg/L]	Augusta station on Skunk river (USGS code: 05474000)	875 days/ 220 days	Daily	-	• **SRC RMSE = 278.77 MAE = 163.19 R = 0.47 • **MLR RMSE = 230.92 MAE = 103.42 R = 0.80 • **SVM-RBF RMSE = 180.76 MAE = 81.09 R = 0.75 • **SVM-PK RMSE = 180.72 MAE = 79.41 R = 0.83 • **LibSVM RMSE = 121.38 MAE = 64.39 R = 0.90 • **NF RMSE = 131.25 MAE = 73.71 R = 0.89	**The best performance from one set of inputs combination

Fathabadi et al., 2022	BLR, GPR, and K-NN/SRC	SSC, Discharge	SSC [mg/L]	Arazkoseh station, Oghan station and Jajrood station in Iran	70% / 30% of available data	Daily	-	• **Arazkoseh BLR NSE = 0.55 BLR R = 0.83 GPR NSE = 0.57 GPR R = 0.76 KNN NSE = 0.59 KNN R = 0.78 • **Oghan BLR NSE = 0.44 BLR R = 0.77 GPR NSE = 0.47 GPR R = 0.74 KNN NSE = 0.52 KNN R = 0.72 • **Jairood BLR NSE = 0.35 BLR R = 0.75 GPR NSE = 0.67 GPR R = 0.84 KNN NSE = 0.66 KNN R = 0.82	-

Appendix B

List of inputs

Table 10 List of inputs (hydrometeorological forcing and static watershed attributes)

Inputs	Product	Variables	Unit	Description
Hydrometeorological Forcing	DAYMET	dayl	s/day	Duration of the daylight period in seconds per day. This calculation is based on the period of the day during which the sun is above a hypothetical flat horizon
		prcp	mm/day	Daily total precipitation in millimeters per day, sum of all forms converted to water-equivalent. Precipitation occurrence on any given day may be ascertained.
		srad	W/m^2	Incident shortwave radiation flux density in watts per square meter, taken as an average over the daylight period of the day. NOTE: Daily total radiation (MJ/m2/day) can be calculated as follows: ((srad (W/m2) * dayl (s/day)) / l,000,000)
		swe	Kg/m^2	Snow water equivalent in kilograms per square meter. The amount of water contained within the snowpack.
		tmax	Deg C	Daily maximum 2-meter air temperature in degrees Celsius.
		tmin	Deg C	Daily minimum 2-meter air temperature in degrees Celsius.
		Vp	Pa	Water vapor pressure in pascals. Daily average partial pressure of water vapor.
Static Watershed Attributes	GAGES-II	ELEV_MEAN_M_BASIN	m	Mean watershed elevation (meters) from 100m National Elevation Dataset
		SLOPE_PCT	-	Mean watershed slope, percent. Derived from 100m resolution National Elevation Dataset, so slope values may differ from those calculated from data of other resolutions.
		DRAIN_SQKM	km^2	Watershed drainage area, sq km, as delineated in our basin boundary

		DEVNLCD06	%	Watershed percent "developed" (urban), 2006
		FORESTNLCD06	%	Watershed percent "forest", 2006
		STREAMS_KM_SQ_KM	km/km^2	Stream density, km of streams per watershed sq km
		MAJ_DDENS_2009	number per 100 km^2	Major dam density
		GEOL_REEDBUSH_DOM_PCT	%	Percentage of the watershed covered by the dominant geology type
		PPTAVG_BASIN	cm	Mean annual precipitation for the watershed
		PERMAVE	inches/hour	Average permeability
		HIRES_LENTIC_DENS	Number per km^2	Density of Lakes/Ponds + Reservoir water bodies
		FRAGUN_BASIN	-	Fragmentation Index of "undeveloped" land in the watershed. High numbers = more disturbance by development and fragmentation; a very pristine basin with a lot of contiguous undeveloped land cover would have a low number
		STOR_NID_2009	ML/km^2	Dam storage in watershed
		MAINS100_FOREST	%	Mainstem 100m buffer "forest"
		MAINS100_DEV	%	Mainstem 100m buffer "developed"
		RRMEAN	-	Relief ratio, calculated as (ELEV_MEAN - ELEV_MIN)/(ELEV_MAX - ELEV_MIN).
		RFACT	100s ft-tonf in/h/ac/yr	Rainfall and Runoff factor ("R factor" of Universal Soil Loss Equation); average annual value for period 1971-2000
		WTDEPAVE	ft	Average value of depth to seasonally high water table
		IMPNLCD06	%	Watershed percent impervious surfaces from 30-m resolution NLCD06 data
		HGA	%	Percentage of soils in hydrologic group A. Hydrologic group A soils have high infiltration rates. Soils are deep and well drained and, typically, have high sand and gravel content.
		HGB	%	Percentage of soils in hydrologic group B. Hydrologic group B soils have moderate infiltration rates. Soils are moderately deep, moderately well drained, and moderately coarse in texture.
		HGC	%	Percentage of soils in hydrologic group C. Hydrologic group C soils have slow soil inflitration rates. The soil profiles include layers impeding downward movement of water and, typically, have moderately fine or fine texture.
		HGD	%	Percentage of soils in hydrologic group D. Hydrologic group D soils have very slow infiltration rates. Soils are clayey, have a high water table, or have a shallow impervious layer.

		AWCAVE	-	Average value for the range of available water capacity for the soil layer or horizon
		TOPWET	ln(m)	Topographic wetness index, ln(a/S); where "ln" is the natural log, "a" is the upslope area per unit contour length and "S" is the slope at that point
		RUNAVE7100	mm/year	Estimated watershed annual runoff
		HYD_DIS_INX	-	Hydrological Disturbance Index based on 7 variables: 1) MAJ_DDENS_2009, 2) WATER_WITHDR, 3) change in dam storage 1950-2009, 4) CANALS_PCT, 5) RAW_DIS_NEAREST_MAJ_NPDES, 6) ROADS_KM_SQ_KM, and 7) FRAGUN_BASIN. Low values = low anthropogenic hydrologic modification in the watershed, high values = high anthropogenic hydrologic modification

Appendix C

Training and Testing period of each site

S_Training: Starting date of training
E_Training: Ending date of training
S_Testing: Starting date of testing
E_Testing: Ending date of testing
no_days: the number of days from the starting date of training to the ending date of testing

Table 11 Training and Testing period for each site

sta_id	S_Training	E_Training	S_Testing	E_Testing	no_days
1127500	19800101	19800805	19800806	19800929	272
1192883	19810228	19870325	19870326	19880929	2770
1197500	19800101	19921231	19930101	19960401	5935
1198125	19940325	19951105	19951106	19960401	738
1331095	19800101	19971018	19971019	20020331	8125
1357500	19990301	20150305	20150306	20190307	7311
1470500	19800101	19810524	19810525	19810929	637
1491000	19801001	19890718	19890719	19910929	4015
1545600	19801001	19810718	19810719	19810929	363
1567000	19800101	19901011	19901012	19930621	4920
1589000	20101001	20140929	20140930	20150929	1824
1589290	20151001	20181212	20181213	20190930	1460
1594440	19841027	19900511	19900512	19910929	2528
1595500	19800214	19800814	19800815	19800929	228
1597000	19800204	19810531	19810601	19810929	603
1603000	19800510	19820407	19820408	19820929	872
1614500	19800101	19800805	19800806	19800929	272
1638500	19800101	19900820	19900821	19930418	4856
1639000	19891001	19921211	19921212	19930929	1459
1642438	20080717	20100704	20100705	20101231	897
1658500	19821001	20051211	20051212	20110929	10590
1659000	20000324	20090609	20090610	20110929	4206
1664000	19800101	19901230	19901231	19930929	5020
2035000	19801001	19810412	19810413	19810531	242
2066000	19800101	19810524	19810525	19810929	637
2075500	19800101	19810524	19810525	19810929	637

2084160	19800101	19851025	19851026	19870409	2655
2116500	19800101	19871018	19871019	19890929	3559
2148315	19831001	19841211	19841212	19850331	547
2269160	20070716	20101106	20101107	20110905	1512
2489500	19800101	19901230	19901231	19930929	5020
3061500	19800101	19810524	19810525	19810929	637
3068800	19800101	19810523	19810524	19810927	635
3111500	19800524	19810622	19810623	19810929	493
3111548	19821208	19891224	19891225	19910929	3217
3150000	19800101	19890524	19890525	19910929	4289
3151400	19800101	19810524	19810525	19810929	637
3187500	19800101	19800804	19800805	19800928	271
3195500	19850201	19861023	19861024	19870330	787
3197000	19850215	19860602	19860603	19860929	591
3201902	19840719	19850421	19850422	19850630	346
3201980	19840809	19850426	19850427	19850630	325
3207800	19800105	19810525	19810526	19810929	633
3209300	19800115	19810501	19810502	19810828	591
3209500	19800306	19810221	19810222	19810521	441
3210000	19800101	19820312	19820313	19820929	1002
3211500	19800303	19820325	19820326	19820929	940
3212500	19800101	19810409	19810410	19810804	581
3216500	19800101	19810405	19810406	19810730	576
3226800	19800101	19810524	19810525	19810929	637
3230450	19921001	20140507	20140508	20190930	9860
3230500	19921112	19970726	19970727	19980929	2147
3234500	19800101	19820312	19820313	19820929	1002
3245500	19800101	19871018	19871019	19890929	3559
3248500	19800101	19810320	19810321	19810710	556
3277500	19800506	19810618	19810619	19810929	511
3280600	19800101	19810524	19810525	19810929	637
3281000	19800101	19810415	19810416	19810811	588
3281100	19800101	19810312	19810313	19810629	545
3281500	19800101	19800425	19800426	19800524	144
3302680	19800101	19800805	19800806	19800929	272
3316500	19801001	19810718	19810719	19810929	363
3319000	19800101	19810415	19810416	19810811	588

3320000	19800101	19810524	19810525	19810929	637
3320500	19800101	19810312	19810313	19810630	546
3328500	19800101	19800805	19800806	19800929	272
3335500	19800101	19800805	19800806	19800929	272
3339000	20110315	20120608	20120609	20120929	564
3347500	19800103	19800806	19800807	19800929	270
3361000	19800101	19810409	19810410	19810803	580
3365500	19800101	19810524	19810525	19810929	637
3382100	19800101	19810524	19810525	19810929	637
3384450	19800101	19810524	19810525	19810929	637
3401000	19800108	19801114	19801115	19810131	389
3402000	19800101	19900313	19900314	19920929	4655
3403500	19800101	19900313	19900314	19920929	4655
3403910	19800125	19810407	19810408	19810726	548
3404000	19800101	19900313	19900314	19920929	4655
3410210	19851001	19860718	19860719	19860929	363
3410500	19831001	19890506	19890507	19900929	2555
4024098	19800101	19810503	19810504	19810902	610
4073462	19811203	20120519	20120520	20191231	13907
4084445	19860702	19891123	19891124	19900929	1550
4086600	19820701	19840417	19840418	19840929	821
4087000	19820701	19840417	19840418	19840929	821
4087030	19820601	19840411	19840412	19840929	851
4087120	19820601	19840411	19840412	19840929	851
4087159	19821001	19840506	19840507	19840929	729
4095300	19900625	19931121	19931122	19940929	1557
4102700	19800424	19820227	19820228	19820815	843
4178000	20170301	20190607	20190608	20191231	1035
4182000	20171220	20190804	20190805	20191231	741
4183000	20180624	20190911	20190912	20191231	555
4183500	20170101	20190526	20190527	20191231	1094
4184500	20181001	20190930	20191001	20191231	456
4186500	20140301	20181030	20181031	20191231	2131
4193500	19800101	19981229	19981230	20030929	8672
4197100	19871001	19890506	19890507	19890929	729
4198000	19800101	19980312	19980313	20020929	8307
4199000	19871001	19901211	19901212	19910929	1459

4200500	19800612	19810414	19810415	19810630	383
4201500	19800101	19810524	19810525	19810929	637
4202000	19850226	19860605	19860606	19860929	580
4206000	19800101	19810524	19810525	19810929	637
4208000	19800101	19980312	19980313	20020929	8307
4209000	19800101	19810524	19810525	19810929	637
4212100	19800101	19890524	19890525	19910929	4289
4233286	20030131	20140105	20140106	20160929	4990
4233300	19981202	20130306	20130307	20160929	6511
5059000	19800101	19800805	19800806	19800929	272
5123400	19890403	19890510	19890511	19890520	47
5275000	19800207	19810510	19810511	19810902	573
5280000	19800104	19810524	19810525	19810928	633
5291000	19800101	19861207	19861208	19880831	3165
5293000	19800101	19861207	19861208	19880831	3165
5304500	19800103	19810417	19810418	19810813	588
5319500	19800208	19800711	19800712	19800819	193
5325000	19800101	20100312	20100313	20170929	13786
5341500	20131001	20150506	20150507	20150929	728
5342000	20131001	20150506	20150507	20150929	728
5357335	19910501	19940122	19940123	19940929	1247
5372995	19810326	19820329	19820330	19820630	461
5385000	19800101	19810524	19810525	19810929	637
5385500	19800101	19810524	19810525	19810929	637
5388250	19800101	19810524	19810525	19810929	637
5389400	19911001	20020222	20020223	20040929	4747
5406500	19841001	19860222	19860223	19860630	637
5416900	20000426	20020404	20020405	20020929	886
5418500	19800101	19991018	19991019	20040929	9038
5419000	19941001	19970222	19970223	19970929	1094
5422000	19960101	19980526	19980527	19990101	1096
5422470	19800101	19810807	19810808	19811231	730
5426000	19800101	19820312	19820313	19820929	1002
5426067	20021029	20040605	20040606	20041030	732
5427718	19900301	20131030	20131031	20190930	10805
5427850	20081001	20170718	20170719	20190930	4016
5427948	19800101	20111231	20120101	20191231	14609

5431016	19930201	20140813	20140814	20191231	9829
5431017	19891001	20131212	20131213	20191231	11048
5431022	19831001	19900222	19900223	19910929	2920
5431486	19800101	19820312	19820313	19820929	1002
5432695	20061001	20140929	20140930	20160929	3651
5432927	20061001	20140929	20140930	20160929	3651
5434500	19800101	19820312	19820313	19820929	1002
5436500	19800101	19850524	19850525	19860929	2463
5438500	20060512	20070620	20070621	20070929	505
5439000	19800101	19810524	19810525	19810929	637
5440000	19800101	19810524	19810525	19810929	637
5446500	19800501	19820405	19820406	19820929	881
5447500	19800101	19810524	19810525	19810929	637
5451500	19880321	19930918	19930919	19950202	2509
5454500	19800101	19860312	19860313	19870929	2828
5455000	19800101	19860312	19860313	19870929	2828
5457000	19800316	19810603	19810604	19810923	556
5465500	19800101	20111018	20111019	20190930	14517
5466500	19800101	19810524	19810525	19810929	637
5471050	19881001	19921212	19921213	19931231	1917
5474000	19800101	20111018	20111019	20190930	14517
5476000	19800101	19810524	19810525	19810929	637
5483450	19800101	19840805	19840806	19850929	2098
5483600	19800101	19840805	19840806	19850929	2098
5498000	19800116	19850527	19850528	19860929	2448
5502500	19880325	19930610	19930611	19940929	2379
5506000	19801129	19820305	19820306	19820629	577
5506500	19821001	19940929	19940930	19970929	5477
5508000	19821001	19880506	19880507	19890929	2555
5516500	19800101	19810524	19810525	19810929	637
5520500	19800101	19921018	19921019	19951231	5843
5525000	19800101	19921018	19921019	19951231	5843
5526000	19800101	19921018	19921019	19951231	5843
5527500	19800101	19921018	19921019	19951231	5843
5527900	20071001	20160718	20160719	20180930	4017
5527905	20071001	20160718	20160719	20180930	4017
5527910	20071001	20170506	20170507	20190930	4382

5536000	19841011	19860508	19860509	19860929	718
5543500	20030201	20080530	20080531	20090929	2432
5548280	19971201	19990210	19990211	19990531	546
5552500	20030218	20080603	20080604	20090929	2415
5555300	19800601	19810624	19810625	19810929	485
5558300	19831001	19910929	19910930	19930929	3651
5567500	19830629	19830910	19830911	19830929	92
5568000	19941001	19970222	19970223	19970929	1094
5568800	19801001	19810718	19810719	19810929	363
5570000	19801001	20071211	20071212	20140929	12416
5570370	19800101	19850806	19850807	19861231	2556
5583000	19801001	19940506	19940507	19970929	6207
5585000	19801001	19940506	19940507	19970929	6207
5587480	20061001	20100929	20100930	20110929	1824
5588720	20000622	20090627	20090628	20110929	4116
5591200	19800101	19940312	19940313	19970929	6481
5594100	19800501	19940406	19940407	19970929	6360
5599500	19800501	19940406	19940407	19970929	6360
6088300	19800101	19820312	19820313	19820929	1002
6088500	19800101	19820312	19820313	19820929	1002
6130500	19821001	19930221	19930222	19950929	4746
6191500	19850507	19910407	19910408	19920929	2702
6192500	19850507	19860619	19860620	19860929	510
6207500	19840301	19840817	19840818	19840929	212
6214500	19800101	19810524	19810525	19810929	637
6236100	19910415	20000426	20000427	20020730	4124
6267400	19800219	19810414	19810415	19810728	525
6268500	19800226	19850604	19850605	19860929	2407
6308500	19800101	19840927	19840928	19851204	2164
6313500	19830503	19840618	19840619	19840929	515
6317000	19830427	19840615	19840616	19840927	519
6324500	19800401	19930612	19930613	19960929	6025
6425720	19800422	19820206	19820207	19820720	819
6441500	20150930	20190223	20190224	20191231	1553
6452000	19811001	20120507	20120508	20191231	13970
6714800	19941018	19960430	19960501	19960917	700
6719505	19810407	19810825	19810826	19810929	175

6758500	19820401	19840422	19840423	19841028	941
6817000	19800101	19900313	19900314	19920929	4655
6906150	19950708	19981124	19981125	19990929	1544
6918070	19910124	19980103	19980104	19990929	3170
7019000	19821006	19851126	19851127	19860909	1434
7036100	19881110	19950303	19950304	19960929	2880
7040100	19850220	19930815	19930816	19950929	3873
7040450	19901001	19940929	19940930	19950929	1824
7046600	19901001	19940929	19940930	19950929	1824
7061270	20060123	20070812	20070813	20080101	708
7061300	20060127	20070813	20070814	20080101	704
7061600	20060127	20070813	20070814	20080101	704
7068510	19800704	19850630	19850701	19860929	2278
7077555	19870403	19900117	19900118	19900930	1276
7103700	19950909	20141207	20141208	20190930	8787
7103970	19970522	20150410	20150411	20190930	8166
7103990	19980408	20091106	20091107	20120929	5288
7104000	19960524	19970515	19970516	19970812	445
7104905	20030403	20160612	20160613	20190930	6024
7105500	19950907	20090501	20090502	20120929	6232
7105530	20130401	20180612	20180613	20190930	2373
7105600	20030401	20101105	20101106	20120929	3469
7105800	19980401	20150612	20150613	20190930	7852
7106300	20140401	20180824	20180825	20190930	2008
7106500	20010531	20160223	20160224	20191031	6727
7124200	19800102	19810422	19810423	19810820	596
7124410	19800101	19831016	19831017	19840927	1731
7126200	19990612	20150908	20150909	20190930	7415
7126300	19851001	19910501	19910502	19920922	2548
7126325	19861020	20130102	20130103	20190723	11964
7126390	19990612	20150714	20150715	20190722	7345
7126415	20020702	20160222	20160223	20190722	6229
7126480	19900710	20121213	20121214	20180724	10241
7126485	19840930	20000825	20000826	20040816	7260
7277700	19860207	20000319	20000320	20030929	6443
7281960	19991001	20021211	20021212	20030929	1459
7281977	19980505	20020830	20020831	20030929	1973

7282000	19961001	19971006	19971007	19980107	463
7287150	19911008	20010507	20010508	20030929	4374
7287160	19911016	20010508	20010509	20030929	4366
7351750	19821001	19860210	19860211	19861214	1535
7352800	19810304	19820801	19820802	19821208	644
8023080	19810202	19840320	19840321	19841231	1428
8023400	19810202	19840810	19840811	19850628	1607
8313000	20080319	20170822	20170823	20191231	4304
8317400	19800101	19861230	19861231	19880929	3194
8329000	20140730	20180911	20180912	20190923	1881
8332010	19800101	20111018	20111019	20190930	14517
8334000	19811001	20120117	20120118	20190815	13832
8353000	19800115	20111015	20111016	20190922	14495
8383000	19800101	19840805	19840806	19850929	2098
8396500	19800101	19900313	19900314	19920929	4655
9041090	19900418	19930120	19930121	19930929	1260
9217000	19800101	19900313	19900314	19920929	4655
9243900	19800327	19810313	19810314	19810609	439
9251000	19800101	19821229	19821230	19830929	1367
9302000	20060421	20080202	20080203	20080714	815
9306500	19851001	19890930	19891001	19900930	1825
9326500	20140501	20180710	20180711	20190728	1914
9364500	19800101	19901230	19901231	19930929	5020
9368000	19800101	19850524	19850525	19860929	2463
9386300	19990710	20151125	20151126	20191230	7478
9397300	19811002	19970920	19970921	20010918	7291
9415000	19921001	19950222	19950223	19950929	1093
9535100	19810110	19810803	19810804	19810924	257
10104700	19860319	19900821	19900822	19910930	2021
10118000	19861001	19940929	19940930	19960929	3651
10174500	19850101	19910314	19910315	19920930	2829
10336610	19800301	19900325	19900326	19920929	4595
10336645	19801001	19900506	19900507	19920929	4381
10336660	19800101	19900313	19900314	19920929	4655
10336676	19800101	19900313	19900314	19920929	4655
10336698	19800101	19840805	19840806	19850929	2098
10336740	19831001	19861211	19861212	19870929	1459

10336780	19800301	19870111	19870112	19880929	3134
11023000	19840101	19840723	19840724	19840912	255
11042000	19831201	19840730	19840731	19840929	303
11046500	19811001	19820718	19820719	19820929	363
11046530	19861207	19880213	19880214	19880601	542
11047300	19831205	19840731	19840801	19840929	299
11048500	19800101	19840405	19840406	19850430	1946
11051500	19811206	19880204	19880205	19890820	2814
11057500	19800101	19800805	19800806	19800929	272
11059300	19830331	19830823	19830824	19830929	182
11074000	19800101	19811229	19811230	19820630	911
11078000	19800108	19870106	19870107	19881006	3194
11106550	19961001	20010719	20010720	20020930	2190
11109000	20041001	20070223	20070224	20070930	1094
11114000	19800108	19831224	19831225	19841220	1808
11119745	19831201	19851104	19851105	19860430	881
11120000	19811201	19820331	19820401	19820430	150
11120510	19811201	19840823	19840824	19850430	1246
11151870	19800101	19831018	19831019	19840929	1733
11162500	19800101	19800805	19800806	19800929	272
11167800	20071101	20100817	20100818	20110430	1276
11169025	20021101	20160725	20160726	20191231	6269
11172175	20031001	20110531	20110601	20130430	3499
11173575	19991001	20100812	20100813	20130430	4960
11176500	20191001	20191212	20191213	20191231	91
11176900	20061001	20170507	20170508	20191231	4839
11177000	19991001	20020905	20020906	20030531	1338
11179000	19991001	20151212	20151213	20191231	7396
11180825	19801201	19981129	19981130	20030531	8216
11180900	19991001	20020905	20020906	20030531	1338
11180960	19800101	19980923	19980924	20030531	8551
11181040	19891001	20131212	20131213	20191231	11048
11376000	19800101	19800430	19800501	19800531	151
11377100	19800101	19800430	19800501	19800531	151
11382000	19801108	19830902	19830903	19840516	1285
11389000	19800101	19800430	19800501	19800531	151
11389500	19800101	19800430	19800501	19800531	151

11391000	19800101	19800430	19800501	19800531	151
11407150	19800101	19901230	19901231	19930929	5020
11417500	20001108	20030914	20030915	20040531	1300
11418000	20010113	20030927	20030928	20040531	1234
11425000	19800101	19800430	19800501	19800531	151
11452500	20121130	20180731	20180801	20191231	2587
11460400	20031001	20051117	20051118	20060531	973
11460600	19891001	19900318	19900319	19900430	211
11460750	20031001	20051117	20051118	20060531	973
11465200	19800101	19850216	19850217	19860531	2342
11465750	20061001	20070318	20070319	20070430	211
11466800	20051001	20071024	20071025	20080430	942
11467000	19800101	19850216	19850217	19860531	2342
11468000	19981001	20020625	20020626	20030601	1704
11469000	20001001	20021117	20021118	20030531	972
11476500	19801001	19810718	19810719	19810929	363
11477000	19800101	19800805	19800806	19800929	272
11481500	19800101	19971111	19971112	20020501	8156
11482500	19800101	19970123	19970124	20010430	7790
11525500	20040505	20060116	20060117	20060621	777
11525530	20051201	20060517	20060518	20060628	209
11525600	19800101	19980312	19980313	20020929	8307
11525630	20041101	20060204	20060205	20060531	576
11525655	19810428	20010712	20010713	20060731	9225
11525670	20051201	20060516	20060517	20060627	208
11525854	20040505	20060217	20060218	20060731	817
11528700	19801201	19820117	19820118	19820430	515
11532500	19801001	19810718	19810719	19810929	363
12041200	19800101	19800217	19800218	19800229	59
12044900	19940930	19960506	19960507	19960929	730
12045500	19940930	19950719	19950720	19950930	365
12048000	19991125	20000729	20000730	20000929	309
12323600	19930301	19950324	19950325	19950929	942
12323750	19930401	19950330	19950331	19950929	911
12324200	19850306	20081030	20081031	20140929	10799
12334550	19850308	20100607	20100608	20160929	11528
12340000	19860714	20100914	20100915	20160929	11035

12340500	19860714	20100914	20100915	20160929	11035
12413470	19931001	19940718	19940719	19940929	363
12413500	19931001	19940718	19940719	19940929	363
12413860	19931001	19940718	19940719	19940929	363
12424000	19981001	20010222	20010223	20010929	1094
12510500	19800101	19800831	19800901	19801031	304
13351000	19921120	19990709	19990710	20010306	3028
14101500	19811001	19830506	19830507	19830929	728
14138850	19800101	19850524	19850525	19860929	2463
14138870	19800105	19850525	19850526	19860929	2459
14138900	19800101	19850210	19850211	19860523	2334
14139800	19800101	19850524	19850525	19860929	2463
14226500	19800527	19800904	19800905	19800930	126
14232500	19800601	19800905	19800906	19800930	121
14240525	20010201	20140601	20140602	20170930	6085
14241500	19801031	20061006	20061007	20130331	11839
14243000	19800518	19831112	19831113	19840926	1592
14309000	19801202	19810423	19810424	19810529	178